

Alkali and Alkaline-Earth Cations in Complex with Small Bioorganic Ligands: Ab Initio Benchmark Calculations and Bond Energy Decomposition

R. López^[a] N. Díaz,^[b] D. Suárez,^[b]*

[a] Dr. R. López

Departamento de Química y Física Aplicadas

Universidad de León

Campus de Vegazana, s/n. 24071. León (Castilla y León) Spain.

[b] Dr. N. Díaz, Dr. D. Suárez

Departamento de Química Física y Analítica

Universidad de Oviedo

Julián Clavería 8. 33006 Oviedo (Asturias) Spain

E-mail: dimas@uniovi.

ABSTRACT

Herein we report a computational database for the complexes of alkali (Li(I), Na(I), K(I)) and alkaline-earth cations (Be(II), Mg(II) and Ca(II)) with 25 small ligands with varying charge and donor atoms (“O”, “N” and “S”) that provides geometries and accurate bond energies useful to analyze metal-ligand interactions in proteins and nucleic acids. The role of the ligand→metal charge transfer, the equilibrium bond distance, the electronegativity of the donor atom, the ligand polarizability, and the relative stability of the complexes are discussed in detail. The interacting quantum atoms (IQA) method is used to decompose the binding energy into electrostatic and quantum mechanical contributions. In addition, bond energies are also estimated by means of multipolar electrostatic calculations. No simple correlation exists between bond energies and structural/electronic descriptors unless the data are segregated by the type of ligand or metal. The electrostatic attraction of some molecules (H₂O, NH₃, CH₃OH) towards the metal cations is well reproduced using their (unrelaxed) atomic multipoles, but the same comparison is much less satisfactory for other ligands (e.g., benzene, thiol/thiolate groups, etc.). Besides providing reference structures and bond energies, the database can contribute to validate molecular mechanics potentials capable of yielding a balanced description of alkali and alkaline-earth metals binding to biomolecules.

Introduction

Eleven metals have been considered together with ten indispensable non-metals in defining the biological periodic system of the elements.^[1] Among these biological essential elements, bulk components like oxygen, carbon, hydrogen, nitrogen, and sulfur coexist with relatively large amounts of metals like sodium, magnesium, potassium, and calcium.^[1b] Thus, first rows alkali and alkaline earth elements are abundant biometals that interact with biologically active molecules to accomplish a myriad of biochemical functions. For example, Na(I) and K(I) are involved in transmembrane transport and signaling, with K(I) mainly located in the intracellular media and Na(I) dominating in the extracellular fluids. In addition, a large group of enzymes requires K(I) or Na(I) for optimal activity. These ions also play a role in nucleic acid folding and catalytic activity.^[2] Lithium is a trace element in biology, but its concentration is intimately connected to the physiological Na(I)/K(I) balance.^[3] It is also important in clinical and pharmacological applications to treat bipolar disorders, Alzheimer's disease or even cancer.^[4] On the other hand, Mg(II) and Ca(II) serve both intra- and extracellular roles. Mg(II) is a cofactor in many enzymatic reactions and it is used to stabilize a variety of protein structures.^[5] Within the cell, Mg(II) acts as a counter ion for the energy-rich ATP and also for nucleic acids.^[6] Ca(II) plays a central role in regulating intracellular processes like glycolysis and gluconeogenesis, ion transport, cell division and growth.^[5] Outside the cells, Ca(II) ions are involved in bone formation, cell adhesion, and blood clotting.^[7] Among the alkaline earth cations, Be(II) is extremely toxic, but it is an indispensable element for a wide variety of applications^[8] so that there is much interest in the search for suitable ligands as antidotes for beryllium poisoning in living organisms.

Experimentally, the interaction of alkali and alkaline earth cations with biologically relevant ligands (amino acids and peptides, nucleosides and nucleotides, simple carbohydrates, etc.) has been characterized using solid state structures and thermodynamic data in aqueous solution.^[9]

In addition, metal interactions with low molecular-weight inorganic (hydroxide, chloride, sulfate, and phosphate) and organic ligands (carboxylates, amines, complexones, etc.) in aqueous solution have been previously reviewed.^[10] From these studies, it is concluded that the properties of weak alkali and alkaline earth metal complexes are mainly controlled by electrostatic binding. The stability of the complexes increases with raising the charge of the metal cations or ligands, the size of the cation being also important. Thus, for a given ligand, the stability trend often follows the sequence $\text{Li(I)} > \text{Na(I)} > \text{K(I)}$ and $\text{Ca(II)} > \text{Mg(II)}$. In contrast, Be(II) complexes present a higher degree of covalent character due to its larger Pauling electronegativity as compared to the other *s*-block elements.^[11] The reported binding affinities of Be(II) follow the trend $\text{carboxylate} > \text{alcohol} > \text{aldehyde} > \text{ester}$.^[12]

Clearly, the stability and other chemical properties of the non-covalent complexes between the alkali or alkali-earth cations and biomolecules are determined by enthalpic and entropic factors, involving metal-ligand interactions, bulk solvation, specific solvent effects, etc. To better understand their relative importance, the measurement of the intrinsic stability of monoligand M-L complexes in terms of experimental thermochemical data would be of particular interest. For some monocationic complexes (*e.g.*, Na(I)-L with $\text{L} = \text{H}_2\text{O}$, CH_3OH , CH_3COCH_3 , etc.), their gas-phase bond energies have been measured,^[13] but the amount of data remains scarce. The detection of doubly-charged M(II)-L complexes in the gas-phase is largely hampered by the strongly favourable Coulomb explosion leading to fragmentation into monocations, especially for Be(II)/Mg(II) complexes. Nevertheless, several groups have managed to study the gas-phase complexes of heavier alkaline-earth cations (Ca(II) , Sr(II) , Ba(II)) with small ligands like water, acetonitrile, formamide, methanol and uraci.l^[14]

In principle, the shortage of experimental thermochemical and structural data for the M-L complexes can be mitigated by quantum chemical calculations that can readily determine the binding preferences of the alkali and alkaline earth cations with different types of ligands.

Indeed many theoretical articles reporting ab initio calculations on M(I)-L or M(II)-L species have been published to date, but most of them consider only one or two metal cations bound to a few ligands. Some authors have examined the trends exhibited by the alkali or alkaline-earth cations in their binding against small neutral ligands (H₂O, NH₃, CH₃NH₂, etc.).^[15] These studies indicate that correlated levels of theory are required to predict reliable bond energies and that polarization and distortion effects can dictate the relative trends in bond energies even though the electrostatic contributions dominate their absolute values. There has been also considerable interest in the cation- π interactions^[16] involving the aromatic side chains of amino acids. The general trend of the computed interaction energies in model complexes is Mg(II)>Ca(II) >Li(I)>Na(I)>K(I),^[17] which correlate with the ligand \rightarrow metal charge transfer. Curiously the cation- π contacts are generally classified as noncovalent interactions,^[18] although other authors have concluded that the interaction between substituted benzenes and divalent Be(II) or Mg(II) cations should be best described as a chemical bond (*i.e.* cation- π bond instead of cation- π interaction).^[19] In aromatic ligand rings including basic groups like the ring nitrogen in the imidazole unit of histidine or the pyridine molecule, the cation- π interaction is replaced by the in-plane contact with the heteroatom. ^[17, 20] Other metal-ligand interactions have been also examined by means of computational methods as those of Li(I), Na(I), and K(I) with a number of polyhydroxyl ligands, considered as models of sugars/carbohydrates.^[21] In this case, the cations maximize the number of M(I) \cdots O interactions with the ligands, but the affinities do not increase proportionally to the number of contacts.

To the best of our knowledge, more systematic benchmark studies examining the stability of the various cations in complex with a broad array of neutral and ionic ligands with different donor atoms are still lacking. The only exception seems to be our previous work^[22] reporting high-level ab initio calculations on monoligand Ca(II) complexes with 24 ligands of biological

relevance, which were employed to assess the performance of DFT methods and to gain further insight into the metal-ligand binding. In this work we report the structures and the gas-phase bond energies of a larger set of M-L complexes, comprising six metal cations (M= Li(I), Na(I), K(I), Be(II), Mg(II) and Ca(II)), 17 different neutral ligands (L= water, methanol, formic acid, acetic acid, formaldehyde, acetone, formamide, acetamide, *N*-methyl acetamide (NMA), methyl acetate, ammonia, methylamine, methanimine, 1H-imidazole, benzene, hydrogen sulphide and methanethiol) and 8 anionic species (hydroxide, methanolate, acetate, imidazolate, hydrosulfide, methanethiolate, formate and methyl phosphate). The set of ligands contains mainly molecules with O donor atoms although other ligands with N and S donors as well as benzene are also included. With respect to the former work on the Ca(II) complexes, we apply an improved protocol in terms of the basis sets and the inclusion of core-valence correlation effects. The resulting bond energies are subject to comparative analysis in order to determine the similarities and differences among the metal cations. In addition, we estimate the magnitude and importance of electrostatic and non-electrostatic effects for a metal-ligand particular interaction by means of the interacting quantum atoms (IQA) technique,^[23] which aims to partition the total energy of a molecular system into atomic and group contributions. Other techniques (*e.g.*, symmetry adapted perturbation theory, SAPT; Ziegler's energy decomposition analysis, etc.) have been used in former studies on metal-ligand complexes to similarly describe the role of electrostatics, charge transfer, induction effects, but herein we pursue the application of IQA to further explore its capability to characterize non-covalent binding.^[24] Overall, our benchmark calculations on the complexes formed between the most common alkali and alkaline-earth metals and the selected ligands would provide a standardized database that can be of great help to outline more robust quantitative trends about the intrinsic binding preferences of the various metal cations as well as to carry out further computational experiments aimed to method development and validation.

Computational Methods

Ab initio calculations

All the ab initio calculations on the metal-ligand complexes studied in this work were performed with full-electron correlation and using the core-valence basis sets (CVXZ, X=T, Q and 5) for the alkali and alkaline earth metals, which have been developed and recommended by Martin and coworkers^[25] for ensuring adequate basis set extrapolation/convergence calculations. In particular, these authors have noticed that inclusion of subvalence correlation is essential for K and Ca, strongly recommended for Na, and optional for the other cations. On the other hand, the aug-cc-pwCVXZ basis sets,^[26] which augment the original Dunning's aug-cc-pVXZ sets by including extra functions designed for core-core and core-valence correlation,^[27] were used for all the non-metal atoms except for the H atoms for which we used the aug-cc-pVXZ set. For the sake of simplicity, herein we will use the notation CVXZ for referring to the basis set employed in the various calculations (*e.g.*, CVTZ stands for CVTZ for the metal cation, aug-cc-pwCVTZ for CNOSP, and aug-cc-pVTZ for H).

Molecular geometries were optimized *in vacuo* at the MP2/CVTZ level and using symmetry constraints in some complexes. MP2/CVTZ analytical Hessian calculations on the optimized geometries confirmed the signature of the critical points as energy minima. To refine the electronic energies, we performed single-point CCSD(T)/CVTZ energy calculations (coupled cluster single and double excitation augmented with a noniterative treatment of triple excitations).^[28] Subsequently, the MP2 correlation energies were extrapolated towards the CBS (complete basis set) limit from MP2/CVXZ ($X = Q, 5$)/MP2/CVTZ energies using a rational extrapolation formula^[29]

$$E_n = E_{CBS} + An^{-3} \quad (1)$$

where n is the cardinal number of the basis set ($n=4$ or 5), and E_{CBS} and A are fitting parameters, with E_{CBS} being the resulting estimate of the CBS limit. The HF energies were not extrapolated, and the CV5Z HF values were taken as the CBS limit. Subsequently, the CBS limit of the CCSD(T) correlation energies was approximated by means of a “composite” formula:

$$E_{composite} = E_{CCSD(T)/CVTZ} + (E_{MP2/CBS} - E_{MP2/CVTZ}) \quad (2)$$

To better assess the influence of the CBS & geometry optimization protocols on the computed bond energies, the geometries of selected M-L complexes with M=Li, Be, Na, Mg, K, Ca and L=H₂O, H₂S, OH⁻ and HS⁻ were reoptimized at the CCSD/CV5Z level followed by single-point CCSD(T)/CVXZ ($X = Q, 5$) calculations that were used to derive CCSD(T)/CBS energies using Eq. (1). In this way, the comparison of the bond energies computed with the composite (Eq. (2)) or the CCSD(T)/CBS electronic energies may yield an estimation of the residual uncertainty of the energetic predictions.

All the MP2 geometry and frequency calculations were carried out with the *Gaussian09* package,^[30] while the CCSD optimizations and all the single-point CCSD(T) calculations were done with the MOLPRO 2009 package.^[31]

IQA calculations

The IQA approach^[23] is an energy decomposition method that relies on the disjoint partitioning of the real space into atomic regions as achieved within the framework of the quantum theory of atoms in molecules (QTAIM). In particular IQA determines both atomic and inter-atomic energy components by direct numerical integration over the atomic basins (Ω_A) that arise from the topological properties of the charge distribution $\rho(\mathbf{r})$. This charge density $\rho(\mathbf{r})$ is readily obtained from the first-order reduced density matrix $\rho_1(\mathbf{r}_1, \mathbf{r}_1')$ as

calculated by electronic structure methods, but IQA demands also the second-order reduced density matrix $\rho_2(r_1, r_2)$ in order to accomplish the decomposition of the $e-e$ repulsion energy.

In the end, the energy of a molecular system is split into physically-meaningful terms:

$$E = \sum_A E_{net}^A + \sum_{A>B} (E_{int,class}^{AB} + E_{int,xc}^{AB}) \dots \quad (3)$$

where $E_{net}^A \equiv E_{net}(\Omega_A)$ is the net electronic energy of atom A that includes the kinetic energy and the potential energy due to nuclei-electron attractions and electron-electron repulsions within Ω_A . The classical interaction energy between atoms A and B in the molecular system collects all the Coulombic potential energy terms (i.e., $E_{int,class}^{AB} = V_{nn}^{AB} + V_{ne}^{AB} + V_{ne}^{AB} + V_{ee,Coul}^{AB}$) while the QM exchange-correlation contributions to the AB interaction are included in $E_{int,xc}^{AB}$. Note that the classical IQA components are distinguished only in the diatomic interaction energies E_{int}^{AB} , but not for the atomic net energies.

In this work IQA is applied to decompose the closed-shell HF energy of the M-L complexes. In the HF method, both $\rho_1(r_1, r_2)$ and $\rho_2(r_1, r_2)$ are computed from the corresponding canonical molecular orbitals. To account for the (minimal) dispersion effects in the HF energies of the M-L complexes, we added the dispersion interaction energies $E_{int,disp}^{AB}$ derived from the third generation dispersion (D3) correction for DFT and HF methods to the rest of the IQA terms.^[32] The D3 method is a pairwise empirical potential inspired on the London formula for the dispersion attraction between two weakly interacting atoms without modifying the charge density. Thus, the D3-corrected IQA decomposition results,

$$E = \sum_A E_{net}^A + \sum_{A>B} (E_{int,class}^{AB} + E_{int,xc}^{AB} + E_{int,disp}^{AB}) \quad (4)$$

To analyze the bond energy of the M-L complexes, we focused on the interacting quantum fragments (IQF) partitioning of the bond energy rather than on the atomic IQA analysis of the absolute energies. To this end, the atomic net energies and the interaction energies among the atoms placed in the ligand are first collected into a single E_{net}^L term. Similarly, the classical, exchange-correlation and dispersion energies between the metal cation and the ligand atoms are grouped into the corresponding $E_{int,class}^{ML}$, $E_{int,xc}^{ML}$ and $E_{int,disp}^{ML}$ terms. Hence, the metal-ligand bond energy ΔE can be expressed as:

$$\Delta E = \Delta E_{net}^M + \Delta E_{net}^L + \Delta E_{int,class}^{ML} + \Delta E_{int,xc}^{ML} + \Delta E_{int,disp}^{ML} \quad (5)$$

To better assess the weight of electrostatic and the non-electrostatic IQA terms, the purely QM and dispersion terms can be grouped into $\Delta E_{xcr}^{ML} = \Delta E_{net}^M + \Delta E_{net}^L + \Delta E_{int,xc}^{ML} + \Delta E_{int,disp}^{ML}$. This exchange-correlation-repulsion (*xcr*) term accounts for all the deformation and QM effects so that the total bond energy (BE) can be formally expressed as the sum of one QM and one classical contribution ($\Delta E = \Delta E_{int,class}^{ML} + \Delta E_{xcr}^{ML}$). The importance of the electrostatic binding, measured by the IQF $\Delta E_{int,class}^{ML}$ term and using the relaxed density of the M-L complex, was further analysed by means of classical electrostatic calculations involving the charge density of the separated (unrelaxed) metal and ligand fragments. To this end, the charge density of the isolated ligand molecules was described in terms of a multicentric multipolar expansion taking the atomic centers as the expansion sites.^[33] A high order expansion ($l=10$) was used and the atomic multipoles were computed in the spherical harmonic formulation by the corresponding integration on the QTAIM atomic basins. Upon translating and rotating the atomic multipoles onto the coordinates of the ligand atoms in the M-L complex, the electrostatic interaction energy, $\Delta E_{int,class}^{M^0L^0}$, between the metal (represented by a zero-order +1.0/+2.0 multipole) and the ligand atoms was evaluated in the spherical tensor formalism as described elsewhere.^[33b] The

comparison between $\Delta E_{\text{int,class}}^{ML}$ and $\Delta E_{\text{int,class}}^{M^0L^0}$ further illustrates the role played by electrostatics and charge-transfer/induction effects.

The decomposition of molecular energies at the HF-D3/CVTZ level was performed with the PROMOLDEN^[34] and the DFTD3^[35] programs. The topology of the charge density is automatically explored by PROMOLDEN prior to the numerical computation of the interatomic surfaces that define the atomic basins Ω_A using a Lebedev angular grid with 5810 points. The IQA quantities are numerically integrated over the atomic basins, which constitute finite and irregular integration domains, using the following settings. First, a spherical region (a β -sphere) contained inside each atomic basin was considered with a radius equal to 60 % the distance of its nucleus to the closest bond critical point in the electron density. Secondly, high-quality Lebedev angular grids were used with 5810 and 974 points outside and within the β -spheres, respectively. Euler-McLaurin radial quadratures were employed with 512 and 384 radial points outside and inside the β -spheres of heavy atoms, respectively (384 and 256 points for H). The largest value of the radial coordinate in the integrations was 15.0 au. Maximum angular moments, λ_{max} , of 10 and 6 were assigned to the Laplace and bipolar expansions of the $1/r_{12}$ operator outside and within the β -spheres.

The PROMOLDEN program also calculates the atomic multipoles in the spherical harmonic formalism up to the λ_{max} order. The set of atomic multipoles and the molecular coordinates were fed to an auxiliary program developed in our laboratory (MPOLINT), which computes then the purely electrostatic interaction between the metal cation and the ligand molecules. In addition, PROMOLDEN was employed to compute the QTAIM (Bader) atomic charge of the metal ion by integrating the first-order MP2/CPVTZ charge density over the corresponding basin.

Results and Discussion

For the sake of brevity, the MP2/CVTZ molecular geometries of the complexes formed between Li(I), Be(II), Na(I), Mg(II), K(I) and Ca(II), and the 25 selected ligands are shown in the Supporting Information (Figure S1). For each complex, the equilibrium distance between the metal and the ligand donor atom(s) and the Bader atomic charge of the metal cation were also included in Figure S1.

Validation and comparison with experimental or previous theoretical data

Before analyzing the energetic trends for all the examined ligands, we validated the consistency of the composite method used in the BE calculations. We selected a small sample of ligands (water, hydrogen sulfide, hydroxide and hydrosulfide) and tested them with each of the six metals of the study. For the resulting complexes, Table 1 collects the BEs and the equilibrium metal-ligand bond distances. In this way, we evaluate the metal binding of both neutral and anionic ligands and considering two donor atoms (O, S) that exhibit a limiting behavior in terms of their charge transfer (Δq) ability.

The bond distances collected in Table 1 show that the CCSD/CV5Z level predicts systematically slightly shorter $M\cdots L$ contacts than MP2/CVTZ by 0.014 Å on average. Similarly, the BEs (D_e) obtained at the CCSD(T)/CBS level, which range from ~10 to ~512 kcal/mol in absolute value, have small differences with those computed by the composite protocol detailed in Methods. The mean unsigned difference (MUD) amounts to 0.19 kcal/mol. The corresponding energy differences moderately depend on the ligand identity. Thus, the MUD values are 0.12, 0.10, 0.35 and 0.21 for the complexes with H₂O, H₂S, OH⁻ and HS⁻, respectively. It turns out that the Ca(II) complexes result in the largest differences between the CCSD(T)/CBS and the composite BEs (MUD=0.49 kcal/mol) followed by those with Be(II) and Mg(II) (MUD=0.16 and 0.15 kcal/mol, respectively). The role of electron correlation is

probably more accentuated for the divalent cations and, consequently, the composite energies related to Ca(II), Be(II) and Mg(II) may have a slightly larger uncertainty than those referred to the monovalent cations. Anyhow, the BEs obtained with the composite protocol perform quite well as compared with the CCSD(T)/CBS values (*e.g.* the relative differences are well below 0.5%) and, therefore, we conclude that, within “chemical accuracy” (~ 1 kcal/mol), the composite BEs can replace either missing experimental or CCSD(T)/CBS data.

Table 1. Bond energies (D_e in kcal/mol) and Unsigned Differences for the Li (I), Be (II), Na (I), Mg (II), K (I) and Ca (II) monoligand complexes with Water, Hydroxide, Hydrogen sulfide and Hydrosulfide obtained with CCSD(T)/CV5Z and the composite method. Equilibrium $M\cdots L$ distances (in Å) are also indicated.

	$M\cdots L^{(a)}$	CCSD(T)/ CBS	Composite Method ^(b)	Unsigned Difference
Ligand		D_e	D_e	
Li (I)				
water	1.842 (1.824)	-34.81	-34.72	0.09
hydrogen sulfide	2.425 (2.409)	-23.42	-23.38	0.04
hydroxide	1.590 (1.576)	-188.42	-188.23	0.19
hydrosulfide	2.159 (2.145)	-152.81	-152.72	0.09
Be (II)				
water	1.493 (1.482)	-145.55	-145.38	0.17
hydrogen sulfide	2.020 (2.012)	-141.95	-141.84	0.11
hydroxide	1.325 (1.314)	-512.54	-512.18	0.36
hydrosulfide	1.832 (1.821)	-455.98	-455.96	0.02
Na (I)				
water	2.227 (2.210)	-24.86	-24.77	0.09
hydrogen sulfide	2.810 (2.792)	-16.23	-16.14	0.08
hydroxide	1.951 (1.936)	-157.64	-157.46	0.18
hydrosulfide	2.496 (2.479)	-133.22	-133.04	0.18
Mg (II)				
water	1.912 (1.899)	-82.83	-82.69	0.14
hydrogen sulfide	2.441 (2.432)	-77.78	-77.67	0.11
hydroxide	1.699 (1.685)	-386.03	-385.74	0.30
hydrosulfide	2.225 (2.215)	-350.21	-350.17	0.04
K (I)				
water	2.611 (2.608)	-17.97	-17.92	0.05
hydrogen sulfide	3.241 (3.243)	-10.54	-10.48	0.06
hydroxide	2.213 (2.202)	-142.17	-141.97	0.19
hydrosulfide	2.827 (2.818)	-115.76	-115.58	0.18
Ca (II)				
water	2.246 (2.225)	-57.36	-57.19	0.17
hydrogen sulfide	2.828 (2.801)	-46.33	-46.15	0.19
hydroxide	1.917 (1.893)	-343.82	-342.96	0.86
hydrosulfide	2.491 (2.454)	-291.29	-290.54	0.75

(a) MP2/CVTZ and CCSD/CV5Z (in parentheses) bond distances.

(b) Using the additive combination of electronic energies (CCSD(T)/CVTZ + MP2/CBS – MP2/CVTZ).

Table 2. Bond energies ($D_o^{(a)}$) in kcal/mol for the Li (I), Be (II), Na (I), Mg (II), K (I) and Ca (II) monoligand complexes. Experimental data from refs. 18 and 49 are also included (numerical values in Italics; reported uncertainties in parentheses).

	Li(I)	Na(I)	K(I)	Be(II)	Mg(II)	Ca(II)
Ligand						
water	-32.77 <i>-32 (2)</i> <i>-34.0</i>	-23.28 <i>-23 (2)</i> <i>-24.0</i>	-16.63 <i>-17.9</i>	-143.05	-80.75	-55.46
methanol	-36.52 <i>-37 (2)</i>	-25.81 <i>-22 (2)</i>	-18.55	-169.69	-94.82	-65.93
formic acid	-40.78	-30.29	-22.91	-188.07	-109.28	-79.69
acetic acid	-41.17	-28.90	-20.97	-200.65	-117.37	-82.75
formaldehyde	-34.59	-25.18	-18.63	-161.69	-91.78	-65.42
acetone	-44.53	-32.74 <i>-31(1)</i>	-24.74	-205.74	-119.35	-87.90
formamide	-48.38	-35.65	-27.15	-213.92	-126.44	-94.21
acetamide	-51.88	-38.27	-29.28	-227.60	-135.34	-101.87
<i>N</i> -methyl acetamide	-54.41	-39.68	-30.42	-237.83	-141.62	-107.18
methyl acetate	-44.27	-31.52	-23.21	-211.08	-120.87	-88.13
ammonia	-37.49	-26.56 <i>-24 (1)</i>	-18.24	-165.83	-96.10	-63.39
methylamine	-39.68	-28.08	-19.36	-182.61	-106.19	-70.68
methanimine	-39.69	-28.51	-20.12	-180.86	-105.22	-70.83
1H-imidazol	-50.59 <i>-50.4(2.4)</i>	-37.18 <i>-33 (1)</i>	-27.35 <i>-26 (1)</i>	-223.47	-134.68	-95.13
benzene	-36.63 <i>-38</i>	-24.31 <i>-21 (1)</i>	-17.70 <i>-18</i>	-224.64	-119.39	-81.83
hydrogen sulfide	-21.74	-14.93	-9.52	-139.64	-75.88	-44.72
methanethiol	-27.32	-19.29	-12.92	-163.99	-92.68	-56.89
hydroxide	-185.59	-155.67	-140.09	-508.60	-383.91	-340.23
methanolate	-179.18	-149.48	-134.46	-508.83	-377.97	-335.83
formiate	-167.76	-144.98	-127.97	-485.63	-369.15	-316.05
acetate	-170.72	-146.94	-129.65	-501.32	-378.63	-324.02
imidazolate- σ	-144.13	-122.75	-107.05	-443.14	-328.71	-265.13
imidazolate- π	-152.28	-128.61	-116.26	-467.63	-340.85	-296.99
hydrosulfide	-151.29	-132.00	-114.81	-453.89	-348.62	-289.39
methanethiolate	-151.75	-132.13	-114.81	-464.83	-355.85	-294.35
methylphosphonate	-271.44	-237.44	-216.87	-748.64	-589.76	-525.59

(a) Using an additive combination of electronic energies (CCSD(T)/CVTZ + MP2/CBS – MP2/CVTZ) and including ZPVE computed at the MP2/CVTZ level.

The bond energies (D_o) are reported in Table 2 for the Li(I), Be(II), Na(I), Mg(II), K(I) and Ca(II) monoligand complexes compared in this study. These BEs correspond now to 0 K data that result from the combination of the zero-point-vibrational-energy (ZPVE) computed from the MP2/CVTZ frequencies with the “composite” electronic D_e energies. In the Supporting

Information, all the ZPVE, MP2/CVTZ, MP2/CBS and CCSD(T)/CVTZ energy components are reported separately and the performance of the MP2/CVTZ, MP2/CBS and CCSD(T)/CVTZ levels is discussed in terms of their mean unsigned percentage “errors” with respect to the composite protocol. For example, we found that the energetic impact of basis set extension from MP2/CVTZ to MP2/CBS is more important than that observed when going from MP2/CVTZ to CCSD(T)/CVTZ and that MP2/CBS can be a compromise situation between accuracy and computational cost.

Before addressing the trends in the computed BEs for the various types of ligands and metals, we briefly compare our results with experimental thermochemical data and with previous theoretical calculations. The experimental BEs are limited to complexes between monovalent cations and neutral ligands. For some of them, experimental 0 K bond energies^[13, 36] are also included in Table 2. Overall, the agreement between experimental and calculated data is quite satisfactory, especially for BEs of the M-water complexes and those of the Li(I)-adducts that differ in ~1 kcal or less. The stability of the cation- π (M-benzene) complexes is also quite well reproduced. Nevertheless, larger differences of ~2-4 kcal/mol arise in the case of the Na(I) complexes with methanol, ammonia and imidazole.

We observed that the bond energies summarized in Table 2 are similar to those previously reported in theoretical studies employing high level ab initio calculations, particularly in the case of the Li(I) and Be(II) complexes. For example, Corral *et. al.*^[15b] have predicted BE values of -32.7, -21.5, -16.2, -141.7, -78.4 and -53.6 kcal/mol for the M-H₂O complexes (M=Li, Na, K, Be, Mg, Ca). Their equivalent values for the metal-ammonia adducts are -37.4, -26.0, -17.7, -164.5, -93.9 and -61.0 kcal/mol. Rao *et. al.*,^[15a] who have studied the microsolvation of mono- and divalent metal cations, give the following BEs for the M-H₂O complexes: -33.6, -24.4, -16.7, -142.2, -80.3 and -53.6 that are obtained with the G3 composite method. CCSD(T)/CBS

benchmark calculations on the cation- π structures for M=Li, Na, Be, Mg have been also performed by Su et. al.,^[18] the BEs amounting to -38.13, -22.95, -223.73 and -116.85 kcal/mol, respectively. Likewise the experimental-theoretical comparison, the differences between our BE values and those reported in previous theoretical works are \sim 1-3 kcal/mol. The larger disparities tend to occur for the complexes with divalent cations, particularly Mg(II) and Be(II), what is not entirely unexpected given that our full electron correlated calculations were carried out with larger basis sets that should account for core-correlation effects in more detail. Nevertheless, this comparative analysis, necessarily limited to a few complexes, as well as the validation data in Table 1 show that our extended data set containing 25 x 6=150 structures does not present sharp discrepancies neither with former theoretical nor with experimental data and that it constitutes a reliable reference for benchmarking and interpretative purposes.

Trends in the calculated bond energies and structures

The BE results reported in Table 2 can help detect and/or illustrate trends in the intrinsic metal-ligand affinity. Of course, some of them merely confirm well-known properties. For example, complexes with anionic ligands present much larger BEs in absolute value than those reported by neutral ligands. It is also true that BEs in absolute value are larger for the Li(I) > Na(I) > K(I) complexes and for Be(II) > Mg(II) > Ca(II). Nevertheless, other subtler trends or effects can be noticed by closer inspection.

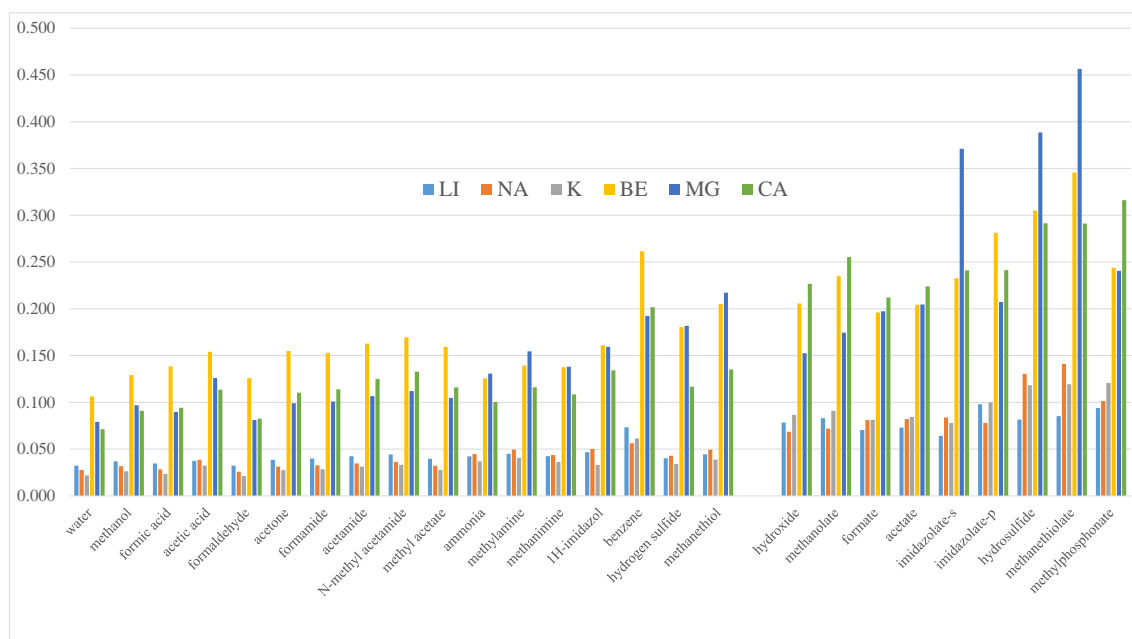
To better characterize the impact on the BEs on going from mono- to divalent cations, we determine first the average quotient of BEs between the Be(II) and Li(I) complexes with neutral ligands and “O/N/S” donor atoms, which have values of 4.6/4.5/6.2, respectively. When anionic ligands are compared, we find similar quotients for the three donor atoms (2.9/3.1/3.0). When we divide the “neutral ligands” quotients by the “anionic ligands” ones, the following comparative ratios are obtained 4.6/2.9 \approx 1.6 for “O”, 4.5/3.1 \approx 1.5 for “N” and 6.2/3.0 \approx 2.0

for “S”. When this comparison is extended to the Na(I) and Mg(II) pair, the comparative neutral to anionic ratios are quite similar now $3.7/2.5 \approx 1.4$ for “O”, $3.7/2.7 \approx 1.4$ for “N” and $4.9/2.6 \approx 1.9$ for “S”. For the K(I) and Ca(II) pair, these equivalent coefficients are $3.5/2.4 \approx 1.5$ for “O”, $3.4/2.5 \approx 1.4$ for “N” and $4.3/2.4 \approx 1.8$ for “S”. From these results, we can obtain two conclusions: (1) deprotonation of ligands in which “S” is the metal-bound atom reinforces metal-binding more significantly than in the case of ligands with “O/N” donor atoms; (2) the ratio of neutral to anionic energy values computed for the same donor atoms maintains a similar value when changing from monovalent to divalent cations, albeit the Li(I) and Be(II) cations tend to discriminate further between neutral and anionic ligands.

When examining the influence of ligand identity on the BE values, we comment first that, among the anionic ligands, OH^- gives the larger BEs in absolute value for all metals except for Be(II), for which is only 0.2 kcal/mol above the BE of CH_3O^- . The small size of OH^- , which can favor stronger ionic contacts with the metal cations, is probably behind this common trend. In general, the BEs of the neutral ligands increase with the donor atom in the order $\text{O} > \text{N} > \text{S}$ although some exceptions arise (*e.g.*, the M- H_2O or M- H_2CO complexes are less stable than M- NH_3 or M- CH_3NH_2). It is also observed that BEs with the SH^- ligand is higher than BEs computed for the HCO_2^- one. Taking into account the relative size, electronegativity and polarizability of the O/N/S atoms, this trend points towards a dominant role played by electrostatics in metal-ligand binding although modulated by other polarization and charge-transfer contributions. For example, among the neutral ligands, *N*-methylacetamide is the most stabilizing ligand for all metals and shows a high charge-transfer according to the Δq values (see below).

The comparison of BEs computed for pairs of similar ligands can be of particular interest. For instance, H₂O and NH₃ result in an unsigned difference (UD) favoring the NH₃ binding of 1.60 kcal/mol for K(I), 3.28 kcal/mol in Na(I) and 4.72 kcal/mol in Li(I), whereas these values rise to 7.33 kcal/mol in Ca(II), 15.35 kcal/mol in Mg(II) and 22.78 kcal/mol in Be(II). In principle the preference for ammonia binding over water should result from the interplay of several factors (metal-ligand equilibrium bond distance, ionic radii, electronegativity of the donor atom) that are better illustrated by the IQA energy decomposition (see below). A similar behavior to that of water/ammonia can be observed for other ligand pairs, such as *N*-methylacetamide and acetamide. On the other hand, when H₂O and H₂S are compared, we observe a different trend in divalent cations, as the energy UD's change to 10.74 kcal/mol in Ca(II), 4.87 kcal/mol in Mg(II) and 3.41 kcal/mol in Be(II) favoring the H₂O binding, that is, Ca(II) is now best at discriminating between H₂O/H₂S ligands (Li(I) presents the larger UD 11.03 kcal/mol among the monovalent cations). This finding may suggest a qualitative change in the mode of binding of the "S" ligands to the divalent cations with respect to the monovalent ones. A similar comparison for the BEs of two anionic ligands, OH⁻ and HS⁻, shows that the UD's favoring OH⁻ binding are clearly larger than those observed for H₂O/H₂S and exhibit peculiar trends: 25.28 kcal/mol in K(I), 23.67 kcal/mol in Na(I), 34.30 kcal/mol in Li(I), 50.84 kcal/mol in Ca(II), 35.29 kcal/mol in Mg(II) and 54.71 kcal/mol in Be(II). Thus, the increment of the Na(I)/Mg(II) BEs upon the HS⁻/OH⁻ exchange are lower than those of K(I)/Ca(II) and Li(I)/Be(II). This finding may indicate that charge-transfer interactions can play a more significant role in these BEs.

Figure 1. Histograms showing the ligand→metal charge transfer (Δq in e^-) computed from the Bader atomic charges and using the MP2/CVTZ density.



A priori, the nature of the metal-ligand binding should be predominantly ionic though some Δq /induction can be also expected. Inspection of the ligand→metal charge transfer (Δq) values can shed some light on the relative importance of these effects. To this end, Figure 1 displays a histogram showing the Δq values derived from the MP2/CVTZ Bader atomic charges. We note in passing that we also computed the Δq values obtained from Natural Population Analysis(NPA) of the MP2/CVTZ density matrix (Figure S2), but the NPA Δq data exhibit a more erratic behavior when sorted out by ligand or metal type than the Bader Δq data, which seem then better suited to outline BE/ Δq trends.

In consonance with expectations, ligand→metal Δq is more accentuated in anionic ligands than in the neutral ones, also in divalent cations with respect to monovalent ones (see $0.206 e^-$ for Be(II)-OH $^-$ vs $0.106 e^-$ for Be(II)-H $_2$ O, $0.082 e^-$ for Li(I)-HS $^-$ vs $0.040 e^-$ for Li(I)-H $_2$ S). Interestingly, complexes with monovalent cations and neutral ligands with “O” as donor atom show a regular Δq trend that increases as Li(I) > Na(I) > K(I) (e.g. $0.037 e^-$ for Li(I)-CH $_3$ OH,

0.032 e^- for Na(I)-CH₃OH, 0.026 e^- for K(I)-CH₃OH). However, when “N” and “S” are the donors, this trend changes to Na(I) > Li(I) > K(I). These trends are not maintained for monovalent cations complexes with anionic ligands (see the Bader charges for Li(I) and Na(I)-anionic ligand complexes in Figure 1).

Of course ligand→metal Δq depends on the metal cation, showing a magnitude of overall 3.3 times higher in divalent metals. When the Δq of the divalent metals are examined in more detail, we find similar values for Mg(II) and Ca(II) in the complexes with neutral ligands and “O” as donor atom, while Be(II) shows a significantly higher Δq (e.g. 0.099 e^- for Mg(II)-C₃H₆O, 0.110 e^- for Ca(II)-C₃H₆O, 0.155 e^- for Be(II)-C₃H₆O). However, we find similar Mg(II) and Be(II) Bader charges, higher than those computed for Ca(II), when donor atoms were “N” and “S”. In anionic complexes, we observe similar Δq values for Be(II) and Ca(II), being Mg(II) significantly lower, when the donor atom was “O”, but significant higher when donor atoms were “N” and “S”. These variations on the metal Bader charges suggest a more pronounced role of ligands (*i.e.*, donor atom hybridization and electronegativity) in their binding to the divalent cations.

In the set of examined ligands, the benzene ring that forms π -cation complexes stands as a unique type of interaction as compared with the rest of neutral complexes, which present a direct σ -interaction between the metal and the donor atom. The nature of π -cation binding is clearly seen in the ligand→metal Δq measured by the Bader methodology so that charge donation by benzene is especially high if it is compared with those of other neutral ligands (see Figure 1). A considerable amount of literature has been published on π -cation interactions and numerous studies have explained the importance of charge-transfer and polarization effects in π -cation complexes.^[16] For example, Zhu *et al.*^[19] have computed the BE for cation-benzene complexes (cation = Li(I), Na(I), K(I), Be(II), Mg(II), Ca(II)) using DFT methods, yielding BE

values which are below our composite values by ~ 2 kcal/mol. By means of the Energy Decomposition Analysis method, they have found a significant non-electrostatic component ($> 50\%$) of the total BE for benzene-cation intermolecular interactions. These results also agree with our previous observations for Ca(II)-benzene complexes.^[22]

For the imidazolate anion, the excess of charge density is equally distributed between the two N atoms while the deprotonated N atom is the only nucleophilic center in the neutral imidazole ring. We found that imidazole forms only π -complexes whereas imidazolate prefers to form distorted π -complexes in which the metal ion lies over the heterocyclic ring, not along the central axis, but closer to the N atoms (see Figure S1). For comparative purposes, we also studied the π -adducts involving one N atom of imidazolate, which turn out to be clearly less stable by ~ 6 -22 kcal/mol depending on the metal cation. However, for Mg(II), K(I) and Ca(II), the planar π -complexes are not stable energy minima on the MP2/CVTZ potential energy surface having a small imaginary frequency ($\sim 50i$ cm⁻¹) for out-of-plane motions.

Finally, we examined the relationship between BEs and a structural parameter like the bond distance r_{M-L} using linear correlation analysis. At view of Table 2 and Figure S1, we find the (BE, r_{M-L}) data to be globally uncorrelated. The highest correlation coefficient (R^2) is 0.800 for K(I)-neutral ligand complexes, the lowest one being 0.398 for Be(II)-neutral ligand complexes. A closer analysis finds some significant correlations if the (BE, r_{M-L}) data are segregated by the donor atom. In this case, the highest R^2 value (0.981) corresponds to the Ca(II)-neutral ligand complexes with “N” as donor but the R^2 is only 0.183 for Ca(II)-neutral ligand complexes with “O” as donor atom. Consequently, the relationship between BE and r_{M-L} is strongly dependent on both the cation and the donor atom. For the sake of completeness, we also studied the relationship between BE and χ_q and between BE and the ligand polarizability. The global (BE, χ_q) data are uncorrelated, but again some significant correlation results in

donor atom subsets. For example, we find R^2 values of 0.953, 0.982 and 0.968 for Li(I), Be(II) and Ca(II), respectively, all cases with “O” as donor atom. We also examined the correlation between BEs and the spherical average polarizabilities (α_{avg}) of the isolated ligand molecules at the MP2/CVTZ level. The global R^2 for the (BE, α_{avg}) sets are similar to those of (BE, α_{q}) and (BE, $r_{\text{M-L}}$), but we observe a stronger correlation involving anionic ligands (*e.g.* R^2 value of 0.901, for Na(I)-anionic ligands for (BE, α_{avg}) sets vs. 0.475 for (BE, α_{q}) and 0.691 for (BE, $r_{\text{M-L}}$) data). A closer inspection also finds significant correlations for neutral ligands when “O” and “N” are the donor atoms (*e.g.* R^2 value of 0.820 (0.982), 0.902 (0.997) and 0.863 (0.992), for Li(I), Be(II) and Ca(II) with “O” (and “N”) as donor atoms respectively).

Bond energy decomposition

From the comparisons of the BE or α_{q} values among the metal-ligand adducts, we can anticipate that electrostatic attraction is most likely the major effect determining the intrinsic stability of the monoligand complexes, what is also in consonance with qualitative expectations. However, it is clear that BE decomposition is required to find out the actual contributions of electrostatic and quantum mechanical effects. Thus, we applied the IQA/IQF methodology to perform such analysis following the conventions and settings described in Computational Methods. To keep the cost of the IQA calculations within reasonable bounds, the BE decomposition is carried out at the HF-D3/CVTZ level, which admits anyway a physical partitioning between electrostatic, exchange-correlation and (empirical) dispersion effects.

Validation of the HF-D3/CVTZ energies

Before carrying out the IQA calculations, we tested the performance of the HF-D3/CVTZ level with reference to the composite protocol. The dispersion correction (D3) was computed with the zero-damping function. Correlation plots and statistical error measures of the HF-D3/CVTZ BEs against the benchmark values are collected in the Supporting Information (Figure S3). The HF-D3/CVTZ BEs are highly correlated to the reference data as the corresponding R^2 values for the divalent cations bound to neutral or anionic complexes are 0.99 while they slightly fluctuate between 0.97-0.99 for the monovalent cations. In terms of the root mean squared (RMS) deviations, the lowest deviations are 0.70 kcal/mol (neutral ligands) and 0.80 kcal/mol (monoanionic) for the K(I) complexes, 2.68 and 2.14 kcal/mol for Ca(II). The largest discrepancy corresponds to the Li(I) and Be(II) complexes for which the RMS values between the HF-D3 and reference data amount to ~ 3 kcal/mol and $\sim 4-5$ kcal/mol, respectively. Taking into account the actual magnitude of the BE, these RMS differences are relatively small. They are also comparable to the errors observed in the DFT-SAPT bond energy calculations for Ca(II) complexes carried out in previous work.^[22]

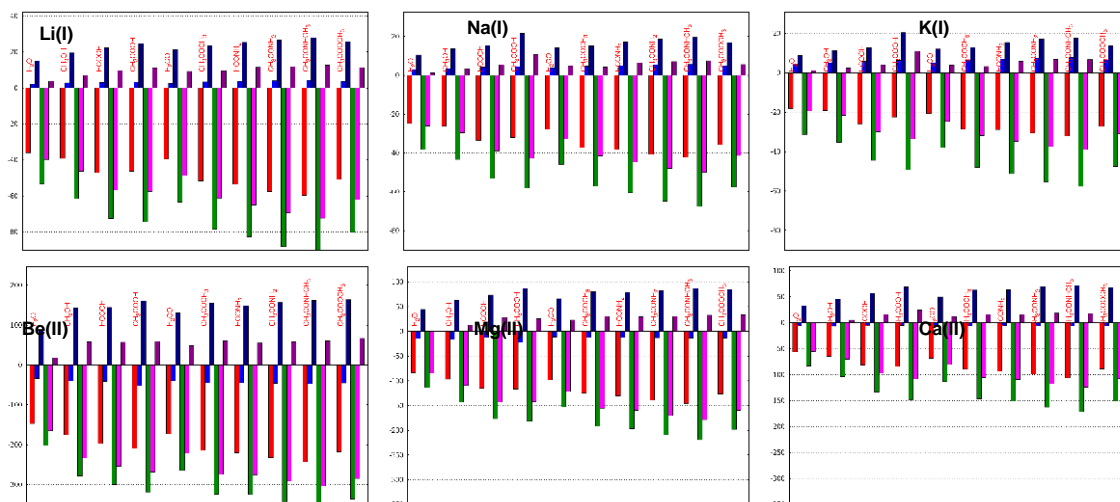
We note in passing that if the popular Becke-Johnson damping function is used in the D3 calculations, instead of the zero-damping option, then the resulting HF-D3(BJ) energies overestimate the BEs. Thus the largest RMS difference between HF-D3(BJ) and composite energies arises in the Be(II) complexes up to ~ 14 kcal/mol, the lowest one corresponding to the K(I) complexes (~ 4 kcal/mol). Although the BJ damping is usually recommended because it reproduces the asymptotic behavior of dispersion energy that tends to a constant contribution at short interatomic distances,^[32] we report only the HF-D3 energies with the original zero damping formulation for the sake of brevity. We note, however, that the D3 correction has only

a minor effect in the computed BEs and that omission of this term has little effect on the magnitude of the HF BEs and on the correlation between HF and ab initio data.

To assess the magnitude of the numerical errors in the IQA quantities, we compared the BEs ΔE^{HF} obtained from the HF-D3 energies and those obtained from the *reconstructed* HF-D3 energies using the IQA terms (ΔE^{IQA}). We found very little difference between the two BEs (*e.g.* MU%E of 0.7% for Li(I), 0.5% for Ca(II); the absolute errors being well below 1 kcal/mol in the majority of the complexes). We conclude then that these small uncertainties, which are caused by the errors produced in the numerical integration carried out by the PROMOLDEN code, would hardly affect the values and relevance of the IQA/IQF descriptors.

Figure 2. Histograms showing the IQA deformation and interaction energy contributions (in kcal/mol) to the HF-D3/CVTZ level bond energies of the metal complexes with neutral ligands. Total formation energy (ΔE^{IOA} from IQA-reconstructed energies in red), fragment deformation energies (ΔE_{def}^M and ΔE_{def}^L in blue and blue-navy, respectively), fragment interaction energies (ΔE_{int}^{ML} in green), Coulombic IQA terms ($\Delta E_{int, class}^{ML}$ in magenta), deformation and exchange-correlation IQA terms and D3 dispersion (ΔE_{scr}^{ML} in dark magenta).

O donor ligands



N/S donor ligands

Li(I)

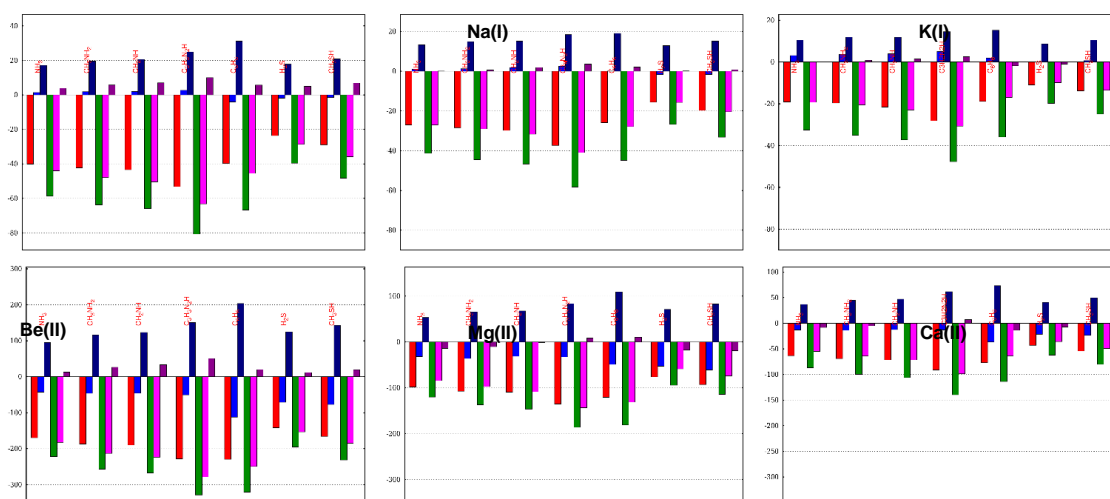
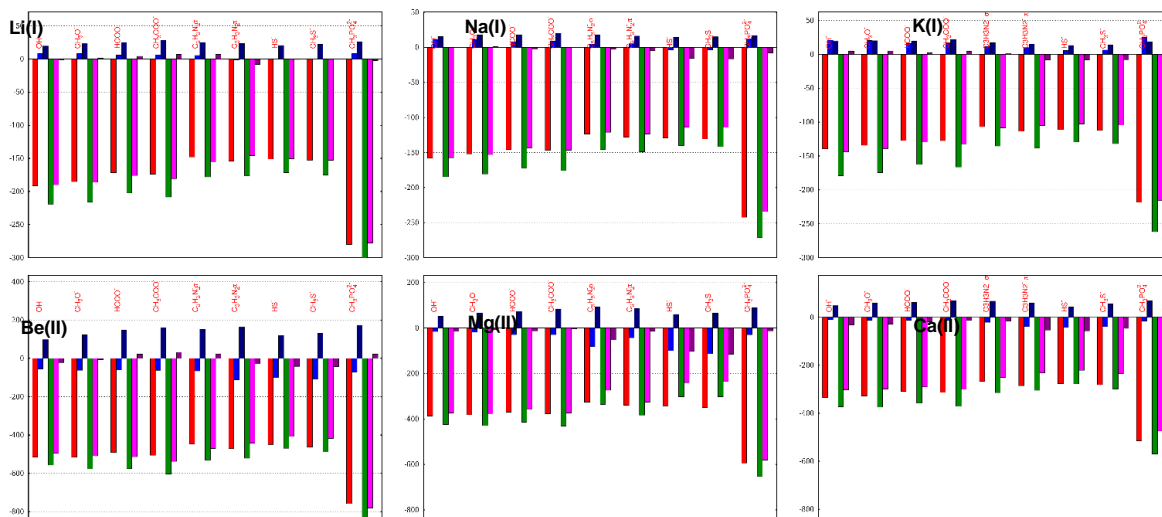


Figure 3. Histograms showing the IQA deformation and interaction energy contributions (in kcal/mol) to the HF-D3/CVTZ level bond energies of the metal complexes with anionic ligands. Total formation energy (ΔE^{IQA} from IQA-reconstructed energies in red), fragment deformation energies (ΔE_{def}^M and ΔE_{def}^L in blue and blue-navy, respectively), fragment interaction energies (ΔE_{int}^{ML} in green), Coulombic IQA terms ($\Delta E_{int,class}^{ML}$ in magenta), deformation and exchange-correlation IQA terms and D3 dispersion (ΔE_{xcr}^{ML} in dark magenta).



Analysis of the IQA/IQF terms

Figures 2 and 3 display the histograms of the IQF terms that result from the decomposition of the HF-D3/CVTZ BEs as defined in equation (5). The numerical values of all the IQA terms are collected in the Supported Information for selected monoligand complexes (Table S3).

One of the IQA advantages is the measurement of the deformation energy of cations and ligands upon complexation. In principle two electronic contributions are collected by the deformation energies, the first one is due to the $\square q$ from the ligand to the metal cation, and the second to the shape deformation of the atomic basin of the metal ion and those in the ligand molecule in passing from their isolated state to the metal-ligand complex, which can be interpreted in terms steric repulsion and electronic polarization.^[37] In addition, the deformation energies of the ligands include also the cost of the geometric strain due to the changes in their internal geometry upon metal binding. We also computed the HF-D3/CVTZ strain energies

(i.e., $\Delta E_{str}^L = E(L^*) - E(L)$ where L^* is the distorted ligand; see Figure S4) and found that they are in general small components of ΔE_{def}^L . For example, the average ΔE_{str}^L values of neutral or anionic ligands (excepting methylphosphonate) complexed with the monovalent ions are 0.9 kcal/mol, well below the average IQA ΔE_{def}^L value of 17.8 kcal/mol. As expected, the geometric distortion induced by divalent cations is stronger and the corresponding mean value of ΔE_{str}^L is 5.7 kcal/mol, but this value is again rather small compared with the average ΔE_{def}^L of 89 kcal/mol. There are, however, some particularities in the strain energies. Thus, the largest values correspond to methylphosphonate, which range from 4 to 48 kcal/mol and constitute a significant 25-40% of the total deformation. It may be also noticed that O-donor ligands tend to be more distorted than the N- or the S-donor ones, and that the bidentate mode of binding of acetic acid or acetate/formiate anions is reflected in a larger strain (see Figure S4). Nevertheless, we conclude that the deformation energy of the ligands, which is always positive (unfavorable for the complex formation), is dominated by their loss of charge density and electronic rearrangement while the geometric strain plays a minor role.

The deformation energies of the metal cations (ΔE_{def}^M) exhibit a more diverse behavior (see Figure 2). For Be(II), its ΔE_{def}^M is negative in all complexes tested, what is in consonance with the relatively large Δq in the Be(II) complexes. A closer inspection shows that the ΔE_{def}^M (in absolute value) is higher in complexes with anionic ligands in accordance with their larger $|\Delta q|$. The same trend is observed in the Mg(II) and Ca(II) complexes although these cations are less stabilized than Be(II) as they accept less charge. In contrast, for the monovalent metals, their ΔE_{def}^M are predominantly positive except for a few combinations in which the most substantial $|\Delta q|$ occurs (see Na(I) or Li(I) with benzene or ligands with “S” as donor atom). This finding indicates that electron repulsion can be more important than the reduction in the net charge in

the monovalent cations when metal-ligand bond is formed. Hence, IQF reveals a qualitative difference in the energetic rearrangements of the monovalent and divalent cations (e.g. $\Delta E_{def}^M = +8.19$ kcal/mol for Li(I)-OH⁻ vs $\Delta E_{def}^M = -55.72$ kcal/mol for Be(II)-OH⁻; $\Delta E_{def}^M = -1.74$ kcal/mol for Na(I)-H₂S vs $\Delta E_{def}^M = -52.89$ kcal/mol for Mg(II)-H₂S).

IQA allows us to estimate the contribution to the total BEs of the electrostatic attraction $\Delta E_{int,class}^{ML}$ involving the *relaxed* densities of the two fragments. Thus, it turns out that some $\Delta E_{int,class}^{ML}$ values are very close to the ΔE^{IQA} values (see Figure 2 and the following examples $\Delta E_{int,class}^{ML} = -150.46$ kcal/mol and $\Delta E^{IQA} = -151.17$ kcal/mol for Li(I)-HS⁻; $\Delta E_{int,class}^{ML} = -152.95$ kcal/mol and $\Delta E^{IQA} = -151.80$ kcal/mol for Na(I)-methanolate, etc.). More particularly, we find rather small differences between $\Delta E_{int,class}^{ML}$ and ΔE^{IQA} for Li(I) complexes with HS[□]/CH₃S[□], Mg(II)-imine, Ca(II)-imine and Na(I) complexes with anionic ligands and “O” donors. Similarly, the $\Delta E_{int,class}^{ML}$ and ΔE^{IQA} values for the Na(I)-NH₃, K(I)-NH₃, Mg(II)-H₂O and Ca(II)-H₂O complexes are very close to each other (differences < 1-2 kcal/mol). Therefore, we see that, for these and other complexes, the IQA decomposition confirms that electrostatics plays a major role since the exchange-correlation and deformation contributions nearly cancel each other. However, we also note that such cancellation of effects is quite variable across the family of metals and ligands examined.

To better assess the weight of the electrostatic and the non-electrostatic IQA terms, we examined the ratio between the total BE ΔE^{IQA} and the ΔE_{xcr}^{ML} quantities. As mentioned in Computational Methods $\Delta E_{xcr}^{ML} = \Delta E_{def}^M + \Delta E_{def}^L + \Delta E_{int,xc}^{ML} + \Delta E_{int,disp}^{ML}$, so that this term can be formally associated to the QM (non-classical) binding effects, while $\Delta E_{int,class}^{ML}$ describes the electrostatic (classical) attraction. Among the neutral ligands, the highest $\Delta E_{xcr}^{ML}/\Delta E^{IQA}$ ratio corresponds to acetic acid (~20-50%), being ΔE_{xcr}^{ML} a repulsive contribution. Excepting the

mono-dentate Li(I)-acetic acid complex, the equilibrium geometries of the cation-acetic acid complexes show a bidentate mode of binding whereas the rest of neutral ligands (including formic acid) result in monodentate structures. This may explain the high $\Delta E_{xcr}^{ML}/\Delta E^{IQA}$ ratios for the acetic acid complexes, which is especially high for the most polarizable cation, K(I), as it reaches a weight of 49.5% in the BE. Other remarkable ΔE_{xcr}^{ML} contributions occur in the complexes with the hydrogensulfide and methanethiolate anionic ligands, but in this case ΔE_{xcr}^{ML} reinforces metal binding and accounts for ~10-30% of the total BE. On the other hand, Li(I) and Be(II) present the highest $\Delta E_{xcr}^{ML}/\Delta E^{IQA}$ ratios of the monovalent and divalent metals, respectively (the mean percentages of non-electrostatic contribution are 13.1% for Li(I) > 10.6% for K(I) > 9.1% for Na(I); 15.5% for Be(II) > 14.4% for Mg(II) > 13.0% for Ca(II)). This trend is in consonance with the top Δq values corresponding to the Li(I) and Be(II) complexes and to the stronger polarization induced by these cations on the ligand atoms given the short metal-ligand distances.

We also analyzed the $\Delta E_{xcr}^{ML}/\Delta E^{IQA}$ ratio when “O” is the donor atom. In this case the QM contributions to BEs are higher for the neutral ligands than for the anionic ones in spite of the Δq values being more important for anionic ligands (*e.g.* Li(I)-formic acid with $\Delta E_{xcr}^{ML}/\Delta E^{IQA} = 20.6\%$ and Δq a of $0.035 e^-$ vs Li(I)-formiate with $\Delta E_{xcr}^{ML}/\Delta E^{IQA} = 2.4\%$ and a Δq of $0.071 e^-$). This shows that, for ligands with “O” donor, the gaining in electrostatic binding is more important than the gaining in QM binding upon deprotonation of the ligands. However, the same comparison for the imidazole/imidazolate, H₂S/HS⁻, CH₃HS/CH₃S⁻ pairs of ligands show a more variable behavior as the weight of non-electrostatics is larger in neutrals only in the Li(I) and Be(II) complexes, suggesting thus a more complex interplay of QM effects involving the metal cation and the ligands.

Interestingly, the Mg(II) cation bound to “O” donor atoms results in the lowest QM contribution to the BE (2.4% for Mg(II) vs 4.1% for Be(II) and 7.1% for Ca(II)) whereas Mg(II) tends to present the highest QM contribution when “N” and “S” are the donor atoms. As above discussed, a parallel trend is appreciated in the Δq values, showing thus that Δq maybe a suitable indicator of the actual importance of CT and polarization in the BEs of the cation-ligand complexes.

The specific binding effects characteristic of benzene are clearly revealed by the exchange-correlation component contribution to the total BE, (i.e., $\Delta E_{xc}^{ML}/\Delta E^{IQA}$). Indeed benzene presents an important, and in most cases predominant, exchange-correlation contribution to the BE (*e.g.* 52.1% for Li(I), 60.3% for Na(I), 88.1% for K(I), 29.9% for Be(II), 38.5% for Mg(II) and 62.0% for Ca(II)) in consonance with the particularly large ligand→metal Δq . This result confirms that CT and polarization effects play an essential role from a quantitative point of view in the cation- π complexes.

In contrast with the cation-benzene structures, the distorted π -complexes given by imidizolate remain largely ionic, the electrostatic term accounting for the majority (>80%) of the cation-imidazolate interaction. This is in consonance with accumulation of negative charge on the ligand N atoms and the asymmetrical positioning of the cation. However, the role of non-classical contributions is still important. Thus, for the second/fourth-row cations, the imidizalote σ -complexes have $\Delta E_{int,class}^{ML}$ values more favorable than those of the counterpart π -structures, but the latter admit a larger charge transfer Δq , which, in turn, stabilize the metal fragment and reinforce the $\Delta E_{int,xc}^{ML}$ energies leading to the more stable π -complexes. Curiously, the Na(I) and Mg(II) π -complexes are favored both by electrostatics and exchange-correlation effects while Δq is larger for the σ -complexes. Hence, IQA suggests that a complex

balance of electrostatic and non-classical effects determines the location of the metal cation around the imidazolate anion.

Another specific ligand effect that is described in depth looking at the IQF descriptors is the NH₃ over H₂O preference in metal binding. This property can be traced back to the lower deformation energy of the metal cation in the M-NH₃ complexes (*e.g.*, for the Na(I)-NH₃ and Na(I)-H₂O pair, $\Delta\Delta E_{def}^M = -1.96$ kcal/mol), which in turn, can be associated to the slightly more important charge transfer $\square q$ induced by NH₃. The NH₃ ligand is more distorted than H₂O, but this variation is compensated by the metal-ligand interaction energy (for Na(I)-NH₃ and Na(I)-H₂O $\Delta\Delta E_{def}^L + \Delta\Delta E_{int}^{ML} = -0.27$ kcal/mol).

It may be interesting to determine the correlation between the ΔE^{HF} BE and the IQA components like $\Delta E_{int,class}^{ML}$. The overall correlation between the wide range of ΔE^{HF} values and the $\Delta E_{int,class}^{ML}$ terms is strong, the highest R^2 values corresponding to the complexes with monovalent metals (R^2 is 0.998 for Li(I), 0.996 for Na(I), 0.997 for K(I), while it is 0.983 for Be(II), 0.967 for Mg(II) and 0.990 for Ca(II)). Again the importance of electrostatics is fully confirmed, but it is also true that the degree of correlation varies significantly on the ligand identity and charge. Thus, the $\Delta E_{int,class}^{ML}$ for neutral ligands have better correlation with BEs than the anionic ones (*e.g.* $R^2 = 0.989$ for Li(I)-neutral ligands, $R^2 = 0.794$ for Be(II)-anionic ligands, etc.). Overall, these R^2 values indicate that Li(I), Na(I) and K(I) are expected to behave more *electrostatically* than the divalent cations (especially for the Be(II)-anionic ligand complexes). We also examined the relationship between $\square q$ and ΔE_{xc}^{ML} , but meaningful correlations only arise if the ($\square q$, ΔE_{xc}^{ML}) data are segregated by the donor atom. In this case, R^2 is over 0.900 for Li(I), Be(II), Mg(II) and Ca(II) with “O” as donor atom and between 0.800 and 0.900 for all donor atoms in these metals. A finer analysis shows some surprising results as in the case of the Be(II)-anionic ligands, in which $R^2=0.246$ for ($\square q$, ΔE_{xc}^{ML}) data, suggesting

thus that it is not feasible to associate the ligand→metal \square q to a given IQA component in exclusive.

Multipolar electrostatic calculations

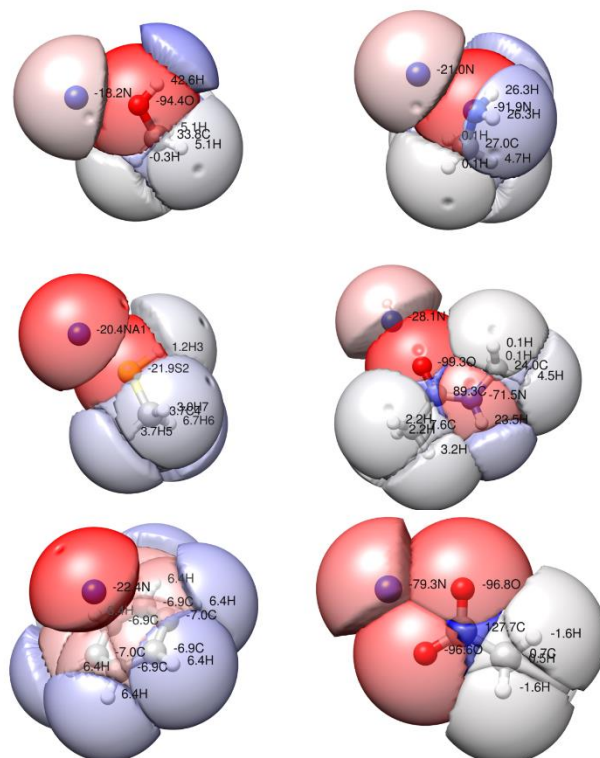
Given the general importance of electrostatic binding in the cation-ligand complexes, we performed classical electrostatic bond energy calculations. As described in Methods, we represented the charge density of the isolated (unrelaxed) ligands by means of distributed multipoles centered on the ligand atoms and taking the equilibrium geometry of the cation-ligand complexes. In this way, the subsequent multipolar calculation allows us to obtain the electrostatic interaction energy (ΔE_{multip}^{ML}) between the metal and the ligand. In this sense, ΔE_{multip}^{ML} accounts for the *purely* electrostatic interactions. Thus, we stress that the ΔE_{multip}^{ML} calculations ignore the QM contributions like polarization, charge transfer and dispersion, but also the classical charge penetration effect (due to the partial overlap of the metal and ligand charge densities).

The ΔE_{multip}^{ML} values are included in Table S2. When we compare the $\Delta E_{int,class}^{ML}$ and ΔE_{multip}^{ML} values for neutral ligands, it turns out that the ΔE_{multip}^{ML} energies in absolute value tend to be below $\Delta E_{int,class}^{ML}$ by several kcal/mol except some complexes with ammonia and methylamine. There are, however, some complexes with a very predominant electrostatic character (*e.g.*, Na(I)-H₂O, Li(I)-methylamine, Mg(II)-NH₃, etc.) that are successfully described by the multipolar expansion given that the differences between $\Delta E_{int,class}^{ML}$ and ΔE_{multip}^{ML} are below 1-2 kcal/mol. Nevertheless, it is also true that differences between $\Delta E_{int,class}^{ML}$ and ΔE_{multip}^{ML} are enhanced as the IQA *xcr* contribution to the total BE becomes more important. Hence, in order to assess to what extent the electrostatic binding in the cation-ligand complexes is modulated by the charge relaxation, we compared the $\Delta E_{int,class}^{ML}/\Delta E^{IQA}$ and $\Delta E_{multip}^{ML}/\Delta E^{IQA}$ ratios. In

these cases, it is clear that the electrostatics in those complexes with a high QM character is not satisfactory described by the multipolar expansion. For example, we obtained $\Delta E_{int,class}^{ML}/\Delta E^{IQA} = 82.8\%$ for Ca(II)-benzene and 90.9% for Ca(II)-imidazol while we obtained $\Delta E_{multip}^{ML}/\Delta E^{IQA} = 55.0\%$ for Ca(II)-benzene and 55.5% for Ca(II)-imidazol.

When anionic ligands are examined, the ΔE_{multip}^{ML} energies overestimate the electrostatic binding measured by the IQF $\Delta E_{int,class}^{ML}$ term, except with Be(II) and Mg(II) with OH⁻ and CH₃O⁻ ligands. The discrepancies between ΔE_{multip}^{ML} and $\Delta E_{int,class}^{ML}$ are larger for anionic ligands than those observed for the neutral ones (up to 15-30 kcal/mol for HS⁻/CH₃S⁻). Again, when we compare the $\Delta E_{int,class}^{ML}/\Delta E^{IQA}$ and $\Delta E_{multip}^{ML}/\Delta E^{IQA}$ ratios for several complexes, we obtain $\Delta E_{int,class}^{ML}/\Delta E^{IQA} = 70.1\%$ for Mg(II)-HS⁻ and 98.1% for K(I)-formiate while we obtained $\Delta E_{multip}^{ML}/\Delta E^{IQA} = 102.3\%$ for Mg(II)-HS⁻ and 108.4% for K(I)-formiate. Hence, the overestimation of the electrostatic interaction by ΔE_{multip}^{ML} may result in a fortuitous agreement with the total QM bond energy for the *softer* ligands.

Figure 4. Ball-and-stick view of Na(I) complexes with methanol, methylamine, methanethiol, N-methylacetamide, benzene and acetate. Atomic labels correspond to the change of additive atomic energies (in kcal/mol) upon complex formation. Atomic basins Ω_A are shown as colored transparent surfaces (blue and red coloring represents destabilized/stabilized atoms, respectively).



Atomic distribution of bond energies

The partitioning of total or relative energies into effective atomic contributions is one of the highest advantages of the IQA approach. To assess the atomic contributions to the BEs of the metal-ligand complexes, we subtract the additive energy of atom Ω_A (with $A \in L$ or $A = M$) in the M-L complex and that in the isolated metal/ligand fragment:

$$\Delta E_{add}^A = E_{add}^{ML}(\Omega_A) - E_{add}^L(\Omega_A)$$

This IQA descriptor becomes useful to evaluate the importance of individual atoms or groups of atoms in the global stabilization of metal-ligand complexes.

The change of additive energies (in kcal/mol) for the metals, ΔE_{add}^A , for selected complexes are shown in Table S3 (ligands considered were methanol, *N*-methylacetamide, methylamine, benzene, methanethiol and acetate). For the sake of clarification, Figure 4 displays a ball-and-stick view of those complexes only for the Na(I) case. To enhance the visual interpretation, the atomic basins \square are shown as colored transparent surfaces, the blue and red colors representing the destabilized/stabilized atoms, respectively. We see in Figure 4 that the metal cation bound to the neutral ligands is largely stabilized by $\Delta E_{add}^M \approx -18-28$ kcal/mol, and that these ΔE_{add}^M represent the major contribution to the total BE. The ligand atoms experience also a notable rearrangement in their ΔE_{add}^A values, but this is much more focused on the donor atoms/functional groups and exhibit both positive and negative changes. For example, the C-OH atoms in Na-methanol undergo an energy change of +44, -94 and 42 kcal/mol (see Figure 4). Hence, the largest ΔE_{add}^A stabilization corresponds to the ligand donor atom, well above that of the metal, but its contribution nearly cancels with the other ΔE_{add}^A values so that the overall change for the methanol molecule is moderate. A similar pattern is observed in methylamine and methylthiol, the C-SH atoms in the latter ligand having less pronounced changes. For the larger *N*-methyl-acetamide ligand, the CNO atoms in the amide functional group exhibit the largest changes, that is, the effect of the metal is localized on the coordinating amide group. In contrast, we observe again a specific pattern in the additive atomic energies for the Na(I)-benzene complex. In this case, the stabilization/destabilization is spread throughout all the C/H atoms in the aromatic ring and the main atomic contribution to the BE is due to the Na(I) cation in contrast with the other neutral ligands. When Table S3 is analyzed in more detail, we observe an intense effect in the ΔE_{add}^M variations in the usual order Li(I) > Na(I) > K(I) for monovalent metals and Be(II) > Mg(II) > Ca(II) for divalent, that is, the IQA

ΔE_{add}^M term reflects the individual role of each metal cations in the enhancement of metal-ligand binding as observed in the composite BEs and in other energetic quantities. Therefore, we conclude that IQA-D3 calculations with the examined level of theory give comparable and consistent results concerning the atomic energy changes.

Conclusions

The ab initio calculations reported in this work have yielded a detailed (energetic, structural and electronic) characterization of the mono-coordinated complexes of alkali and alkaline-earth cations with small ligands. The uncertainty of the computed bond energies (~ 0.1 - 0.5 kcal/mol) has been addressed by comparing the energies produced by various methods and protocols and the consistency of the dataset has been confirmed by comparison with experimental data and former theoretical calculations that are available only for a reduced subset of complexes. In fact, many of the calculated gas-phase energies have not been experimentally studied yet and, therefore, our calculations provide a reliable database that not only significantly augments the number of examined M(I)/M(II)-L structures, but also quantify various trends governing the intrinsic affinities of metal cations for small molecules and functional groups of biological interest.

Examination of the computed bond energies and distances together with the ligand \rightarrow metal charge transfer has allowed us to outline various relationships between metal/ligand identity and the relative stability of the complexes. Some of them have been discussed in detail (*e.g.*, the ratio of neutral to anionic bond energy values computed for the same donor atoms maintains a similar value when changing from monovalent to divalent cations) and other trends could be obtained by performing similar cross-comparisons. Nevertheless, our benchmark dataset indicates that no simple correlation exists between bond energies and structural/electronic descriptors unless the data are segregated by the type of ligand or metal (*e.g.*, O-donor, anionic,

etc.). This and other similar observations point out that the strength of the metal-ligand binding would be modulated by both strong electrostatic attractions and QM effects linked to the donor atom electronegativity, ligand polarizability, etc.

The decomposition of the bond energies following the IQA/IQF formalism gives both qualitative and quantitative insight into the relative importance of electrostatic (classical) and non-electrostatic interactions between the metal cations and the neutral or ionic ligands. Due to the large computational cost of the IQA calculations, the energy partitioning has been achieved at the HF-D3/CVTZ level after having carefully assessed its accuracy and numerical uncertainty. The major role played by electrostatics is clearly shown in the magnitude of the $\Delta E_{int,class}^{ML}$ terms and their correlations with the total BE values. More interestingly, the IQF results reveal the different behavior of M(I) and M(II) in terms of the ΔE_{def}^M values, the actual impact of QM exchange-correlation interactions in the BE, the peculiarities of the cation- π interactions, the atomic distribution of bonding energies, *etc.* When the IQF $\Delta E_{int,class}^{ML}$ energy is compared with the purely electrostatic interaction energy between the metal cation and the ligand (represented by a multicentered multipolar expansion), the extension of the partial (or nearly-total) cancellation of QM effects can be assessed on a particular basis for each metal-ligand combination. In this respect, the electrostatic attraction of some molecules (H₂O, NH₃, CH₃OH) towards the metal cations is quite well reproduced using their (unrelaxed) atomic multipoles, supporting thus the use of empirical electrostatic potentials, but the same comparison is much less satisfactory for other ligands (*e.g.*, benzene, thiol/thiolate groups, etc.) for which the bonded approach (*i.e.*, inclusion of explicit metal-ligand bonds) could be more adequate. Overall, the high level ab initio calculations and the insight offered by the IQA analysis may contribute to validate or to formulate molecular mechanics potentials capable of yielding a balanced description of alkali and alkaline-earth metals binding to biomolecules.

Acknowledgements

This research was supported by the CTQ2015-65790-P and the PGC2018-095953-B grants (MICINN, Spain). We also acknowledge the IDI/2018/000177 (FICYT, Spain) grant. The authors are also indebted to A. Martín-Pendás for his critical reading of the manuscript and E. Francisco for his MPOLINT code.

Supporting materials

Table S1 with bond energies obtained with the MP2 and CCSD(T) methods. Table S2 with the IQA/IQF fragment contributions to the bond energies and classical electrostatic interaction energies for the different systems. Table S3 with IQA atomic additive energy contributions to bond energies for selected complexes. Figure S1 with a ball-and-stick representation of all the metal-ligand complexes optimized at the MP2/CVTZ level. Figure S2 with MP2/CVTZ NPA charge transfer values. Figure S3 showing the comparison between the HF-D3/CVTZ bond energies and the composite values. Figure S4 with HF-D3/CVTZ strain energies of the ligand molecules. ZIP file containing the Cartesian coordinates of all the structures examined in this work.

Keywords: Ab initio calculations • Bond theory • Computational Chemistry • Noncovalent interactions • Quantum Chemistry

References

- [1] a) S. M. Yannone, S. Hartung, A. L. Menon, M. W. Adams and J. A. Tainer, *Current Opinion in Biotechnology* 2012, 23, 89-95. ; b) W. Maret, *Int. J. Mol. Sci.* 2016, 17, 66.
- [2] a) M. Vašák and J. Schnabl, *Met. Ions Life Sci.* 2016, 16, 259-290. ; b) P. Auffinger, L. D'Ascenzo and E. Ennifar, *Met. Ions Life Sci.* 2016, 16, 167-201.
- [3] Y. Kim, T.-T. T. Nguyen and D. G. Churchill, *Met. Ions Life Sci.* 2016, 16, 1-10.

[4] a) D. Mota de Freitas, B. D. Leverson and J. L. Goossens, *Met. Ions Life Sci.* 2016, 16, 557-584. ; b) E. Eric Jakobsson, O. Argüello-Miranda, S.-W. Chiu, Z. Fazal, J. Kruczek, S. Nunez-Corrales, S. Pandit and L. Pritchett, *J Membrane Biol* 2017, 250, 587-604.

[5] T. Dudev and C. Lim, *Chem. Rev.* 2003, 103, 773-787.

[6] W. Jahnen-Dechent and M. Ketteler, *Clin Kidney J* 2012, 5, i3-i14.

[7] J. Evenäs, M. A. and S. Forsén, *Current Opinion in Chemical Biology* 1998, 2, 293-302.

[8] L. C. Perera, O. Raymond, W. Henderson, P. J. Brothers and P. G. Plieger, *Coordination Chemistry Reviews* 2017, 352, 264-290.

[9] a) M. M. Harding, M. W. Nowicki and M. D. Walkinshaw, *Crystallography Reviews* 2010, 16, 247-302. ; b) K. Aoki, K. Murayama and N.-H. Hu, *Met. Ions Life Sci.* 2016, 16, 27-101. ; c) F. Crea, C. De Stefano, C. Foti, G. Lando, D. Milea and S. Sammartano, *Met. Ions Life Sci.* 2016, 16, 133-166.

[10] P. G. Daniele, C. Foti, A. Gianguzza, E. Prenesti and S. Sammartano, *Coordination Chemistry Reviews* 2008, 252, 1093-1107.

[11] K. J. Iversen, S. A. Couchman, D. J. D. Wilson and J. L. Dutton, *Coordination Chemistry Reviews* 2015, 297-298, 40-48.

[12] M. Müller and M. R. Buchner, *Angew. Chem. Int. Ed.* 2018, 57, 9180-9184.

[13] M. T. Rodgers and P. B. Armentrout, *Mass Spectrometry Reviews* 2000, 19, 215-247.
10.1002/1098-2787(200007)19:4<215::aid-mas2>3.0.co;2-x

[14] a) M. Kohler and J. A. Leary, *J. Am. Soc. Mass Spectrom.* 1997, 8, 1124-1133.
10.1016/s1044-0305(97)00155-4; b) A. A. Shvartsburg and K. W. M. Siu, *Journal of the American Chemical Society* 2001, 123, 10071-10075. 10.1021/ja011267g; c) A. Eizaguirre, O.

Mó, M. Yáñez, J.-Y. Salpin and J. Tortajada, *Organic & Biomolecular Chemistry* 2012, *10*, 7552-7561. 10.1039/C2OB26166A; d) C. Trujillo, A. M. Lamsabhi, O. Mó, M. Yáñez and J.-Y. Salpin, *International Journal of Mass Spectrometry* 2011, *306*, 27-36. <https://doi.org/10.1016/j.ijms.2011.05.018>; e) I. Corral and M. Yáñez, *Physical Chemistry Chemical Physics* 2011, *13*, 14848-14864. 10.1039/C1CP20622B

[15] a) J. S. Rao, T. C. Dinadayalane, J. Leszczynski and G. N. Sastry, *The Journal of Physical Chemistry A* 2008, *112*, 12944-12953. 10.1021/jp8032325; b) I. Corral, O. Mó, M. Yáñez and L. Radom, *The Journal of Physical Chemistry A* 2005, *109*, 6735-6742. 10.1021/jp051052j

[16] J. C. Ma and D. A. Dougherty, *Chemical Reviews* 1997, *97*, 1303-1324. 10.1021/cr9603744

[17] A. S. Reddy and G. N. Sastry, *J. Phys. Chem. A* 2005, *109*, 8893-8903.

[18] H. Su, Q. Wu, H. Wang and H. Wang, *Phys. Chem. Chem. Phys.* 2017, *19*, 26014.

[19] W. Zhu, X. Tan, J. Shen, X. Luo, F. Cheng, P. C. Mok, R. Ji, K. Chen and H. Jiang, *J. Phys. Chem. A* 2003, *107*, 2296-2303.

[20] S. Ullah, P. A. Denis and F. Sato, *Computational and Theoretical Chemistry* 2019, *1150*, 57-62.

[21] S. Abirami, N. L. Ma and N. K. Goh, *Chemical Physics Letters* 2002, *359*, 500-506.

[22] D. Suárez, V. M. Rayón, N. Díaz and H. Valdés, *The Journal of Physical Chemistry A* 2011, *115*, 11331-11343. 10.1021/jp205101z

[23] M. A. Blanco, A. Martín Pendás and E. Francisco, *J. Chem. Theory Comput.* 2005, *1*, 1096-1109.

[24] D. Suárez, N. Díaz, E. Francisco and A. Martín Pendás, *ChemPhysChem* 2018, 19, 973-987. doi:10.1002/cphc.201701021

[25] M. A. Iron, M. Oren and J. M. Martin, *Mol. Phys.* 2003, 101.

[26] K. A. Peterson and T. H. Dunning, *J. Chem. Phys.* 2002, 117. 10.1063/1.1520138

[27] a) D. E. Woon and T. H. Dunning, *J. Chem. Phys.* 1993, 98. 10.1063/1.464303; b) R. A. Kendall, T. H. Dunning and R. J. Harrison, *J. Chem. Phys.* 1992, 96. 10.1063/1.462569; c) T. H. Dunning, *J. Chem. Phys.* 1989, 90. 10.1063/1.456153

[28] K. Raghavachari, G. W. Trucks, J. A. Pople and M. Head-Gordon, *Chem. Phys. Lett.* 1989, 157, 479-483

[29] A. Halkier, T. Helgaker, P. Jørgensen, W. Klopper, H. Koch, J. Olsen and A. K. Wilson, *Chemical Physics Letters* 1998, 286, 243-252.

[30] M. J. Frisch, G. W. Trucks, H. B. Schlegel, G. E. Scuseria, M. A. Robb, J. R. Cheeseman, G. Scalmani, V. Barone, B. Mennucci, G. A. Petersson, H. Nakatsuji, M. Caricato, X. Li, H. P. Hratchian, A. F. Izmaylov, J. Bloino, G. Zheng, J. L. Sonnenberg, M. Hada, M. Ehara, K. Toyota, R. Fukuda, J. Hasegawa, M. Ishida, T. Nakajima, Y. Honda, O. Kitao, H. Nakai, T. Vreven, J. A. Montgomery Jr., J. E. Peralta, F. Ogliaro, M. J. Bearpark, J. Heyd, E. N. Brothers, K. N. Kudin, V. N. Staroverov, R. Kobayashi, J. Normand, K. Raghavachari, A. P. Rendell, J. C. Burant, S. S. Iyengar, J. Tomasi, M. Cossi, N. Rega, N. J. Millam, M. Klene, J. E. Knox, J. B. Cross, V. Bakken, C. Adamo, J. Jaramillo, R. Gomperts, R. E. Stratmann, O. Yazyev, A. J. Austin, R. Cammi, C. Pomelli, J. W. Ochterski, R. L. Martin, K. Morokuma, V. G. Zakrzewski, G. A. Voth, P. Salvador, J. J. Dannenberg, S. Dapprich, A. D. Daniels, Ö. Farkas, J. B. Foresman, J. V. Ortiz, J. Cioslowski and D. J. Fox in *Gaussian 09, Vol.* Gaussian, Inc., Wallingford, CT, USA, 2009.

[31] H.-J. Werner, P. J. Knowles, R. Lindh, F. R. Manby, M. Schütz, P. Celani, T. Korona, A. Mitrushenkov, G. Rauhut, T. B. Adler, R. D. Amos, A. Bernhardsson, A. Berning, D. L. Cooper, M. J. O. Deegan, A. J. Dobbyn, F. Eckert, E. Goll, C. Hampel, G. Hetzer, T. Hrenar, G. Knizia, C. Köppl, Y. Liu, A. W. Lloyd, R. A. Mata, A. J. May, S. J. McNicholas, W. Meyer, M. E. Mura, A. Nicklass, P. Palmieri, K. Pflüger, R. Pitzer, M. Reiher, U. Schumann, H. Stoll, A. J. Stone, R. Tarroni, T. Thorsteinsson, M. Wang and A. Wolf in *MOLPRO, version 2009.1, a package of ab initio programs, Vol.*

[32] S. Grimme, A. Hansen, J. G. Brandenburg and C. Bannwarth, *Chemical Reviews* 2016, *116*, 5105-5154. 10.1021/acs.chemrev.5b00533

[33] a) A. J. Stone, *Chem. Phys. Lett.* 1981, *83*, 233-239. ; b) M. Rafat and P. L. A. Popelier, *The Journal of Chemical Physics* 2006, *124*, 144102. 10.1063/1.2186993

[34] A. M. Pendas and E. Francisco in *PROMOLDEN: A QTAIM /IQA code, Vol.* Unpublished, 2015.

[35] S. Grimme, J. Antony, S. Ehrlich and H. Krieg, *The Journal of Chemical Physics* 2010, *132*, 154104. 10.1063/1.3382344

[36] E. López, J. M. Lucas, J. de Andrés, M. Albertí, J. M. Bofill, D. Bassi and A. Aguilar, *Physical Chemistry Chemical Physics* 2011, *13*, 15977-15984. 10.1039/C1CP21889A

[37] E. Francisco and A. Martín Pendás in *Chapter 2 - Energy Partition Analyses: Symmetry-Adapted Perturbation Theory and Other Techniques, Vol.* Eds.: A. Otero de la Roza and G. A. DiLabio), Elsevier, 2017, pp. 27-64.

Comparison between the various levels of theory

In Table S1 the “benchmark” data are the “composite” D_e values. Since the BE range covered by these calculations is on the hundreds of kcal/mol, we resort to the mean unsigned percentage “errors” (MU%E) to assess the relative performance of the MP2/CVTZ energies with respect to the composite values. Thus, the U%E stands in the range 0.8%-2.8% for Li(I), 0.7%-1.9% for Be(II), 0.8%-4.7% for Na(I), 0.7%-2.6% for Mg(II), 2.1%-7.6% for K(I) and 0.0%-3.9% for Ca(II). We also obtain MU%Es for the MP2/CVTZ level of 1.7% for Li(I), 1.2% for Be(II), 2.9% for Na(I), 1.6% for Mg(II), 1.1% for K(I) and 3.1% for Ca(II), with 1.9% as the average error with all metals calculations. The largest errors arise in the metal-benzene complexes (*e.g.*, U%E = 7.6% for K(I)-benzene) so that removal of benzene from the data set leads to a MU%E of only 0.4%. A close inspection also indicates that the MP2-composite MU%Es for neutral ligands are higher than those obtained with anionic ligands except for K(I). When we examine MP2/CBS BEs, the MU%Es for neutral ligands can be found higher than complexes formed with anionic ones only when “O” is the donor atom while “N” and “S” behavior as donor atoms present erratic trends. We can also report MU%Es of MP2/CBS level of 0.6% for Li(I), 0.5% for Be(II), 0.5% for Na(I), 0.4% for Mg(II), 0.8% for K(I) and 0.4% for Ca(II), with 0.5% as average of previous errors. Finally, when comparing the CCSD(T)/CVTZ with the composite BEs, the corresponding MU%Es for neutral ligands errors are higher than those for anionic for all the donor atoms tested. We also report MU%Es of CCSD(T)/CVTZ level of 1.1% for Li(I), 0.7% for Be(II), 2.5% for Na(I), 1.2% for Mg(II), 1.3% for K(I) and 3.4% for Ca(II), resulting an average CCSD(T)/VTZ error of 1.7%. In view of these results, we conclude: (1) improvement in energy calculations caused from the basis set extension is more important than that observed when going from MP2/CVTZ to CCSD(T)/CVTZ. As overall, ongoing from MP2/CVTZ to MP2/CBS reduces errors in BEs by a factor of 4, while the extension only in method accuracy but not in the basis set size, MP2/CVTZ to CCSD(T)/CVTZ, reports similar results (1.9% vs 1.7%). (2) BEs computed at the MP2/CBS level of theory result in similar uncertainties for all metals tested, with a very little 0.5% average error. Consequently, we find MP2/CBS to be in a compromise situation between accuracy and computational cost. (3) BEs for all the neutral complexes here studied with “O” as donor atom present higher errors than those obtained for anionic complexes. It is not possible to report a similar finding for “N, S” as donor atoms as the BE show erratic trends in these cases.

Table S1. Bond energies (in kcal/mol) for the Li (I), Be (II), Na (I), Mg (II), K (I) and Ca (II) monoligand complexes obtained with the MP2 and CCSD(T) methods^(a).

Ligand	MP2/ CVTZ D_e	ZPVE	CCSD(T)/ CVTZ D_e	MP2/ CBS ^(b) D_e	Composite Method ^(c) D_e
Li (I)					
water	-33.98	1.95	-34.06	-34.64	-34.72
methanol	-37.52	1.60	-37.56	-38.09	-38.13
formic acid	-41.35	1.66	-41.83	-41.96	-42.44
acetic acid	-41.31	1.29	-41.89	-41.87	-42.45
formaldehyde	-35.21	1.63	-35.63	-35.80	-36.22
acetone	-44.91	1.42	-45.35	-45.51	-45.95
formamide	-49.38	2.24	-49.99	-50.01	-50.62
acetamide	-52.92	2.27	-53.53	-53.54	-54.15
<i>N</i> -methyl acetamide	-55.25	2.10	-55.89	-55.87	-56.51
methyl acetate	-44.56	1.46	-45.17	-45.12	-45.73
ammonia	-39.35	2.46	-39.43	-39.86	-39.95
methylamine	-41.22	2.07	-41.34	-41.63	-41.75
methanimine	-41.19	2.02	-41.21	-41.69	-41.71
1H-imidazol	-51.22	1.69	-51.44	-52.06	-52.29
benzene	-38.36	2.01	-38.50	-38.50	-38.65
hydrogen sulfide	-23.05	1.65	-23.07	-23.37	-23.38
methanethiol	-28.18	1.29	-28.23	-28.56	-28.61
hydroxide	-185.77	2.65	-187.07	-186.92	-188.23
metoxi	-181.30	3.58	-181.70	-182.36	-182.76
formiate	-168.07	2.40	-168.95	-169.28	-170.16
acetate	-171.05	2.29	-171.78	-172.27	-173.01
imidazolate- σ	-143.59	1.67	-144.69	-144.71	-145.80
imidazolate- π	-152.96	2.43	-153.62	-154.05	-154.71
hydrosulfide	-151.44	1.43	-151.81	-152.35	-152.72
methanethiolate	-152.06	1.61	-152.42	-153.00	-153.36
methylphosphonate	-271.61	2.87	-272.63	-273.29	-274.31

(a) Molecular geometries were optimized at the MP2/CVTZ level.

(b) Obtained from CBS extrapolation of the MP2 correlation energy based on Eq. (1) and using the HF/CV5Z energies.

(c) Using an additive combination of electronic energies (CCSD(T)/CVTZ + MP2/CBS – MP2/CVTZ).

Table S1. (cont.)

Ligand	MP2/ CVTZ	ZPVE	CCSD(T)/ CVTZ	MP2/ CBS^(b)	Composite Method^(c)
	D_e		D_e	D_e	D_e
Be (II)					
water	-143.47	2.33	-143.71	-145.14	-145.38
methanol	-169.16	1.41	-169.69	-170.57	-171.10
formic acid	-187.31	2.51	-188.73	-189.16	-190.58
acetic acid	-198.13	0.68	-199.42	-200.03	-201.33
formaldehyde	-161.22	2.52	-162.50	-162.93	-164.21
acetone	-203.83	1.20	-205.00	-205.77	-206.94
formamide	-213.50	3.37	-215.42	-215.38	-217.29
acetamide	-227.28	3.22	-228.93	-229.16	-230.82
<i>N</i> -methyl acetamide	-237.11	2.82	-238.77	-238.98	-240.65
methyl acetate	-209.55	1.73	-211.07	-211.29	-212.81
ammonia	-167.18	3.01	-167.43	-168.59	-168.84
methylamine	-183.19	2.25	-183.66	-184.40	-184.86
methanimine	-181.54	2.82	-182.08	-183.13	-183.68
1H-imidazol	-221.58	2.29	-223.77	-223.58	-225.76
benzene	-224.81	2.65	-226.07	-226.04	-227.30
hydrogen sulfide	-140.30	2.20	-141.01	-141.13	-141.84
methanethiol	-163.56	1.44	-164.54	-164.45	-165.43
hydroxide	-506.71	3.58	-509.24	-509.65	-512.18
metoxi	-510.44	5.30	-511.43	-513.14	-514.13
formiate	-483.99	3.57	-486.57	-486.61	-489.20
acetate	-499.74	3.27	-501.93	-502.40	-504.59
imidazolate- σ	-437.98	2.22	-442.85	-440.50	-445.37
imidazolate- π	-465.94	3.43	-468.63	-468.37	-471.06
hydrosulfide	-452.94	2.07	-454.50	-454.39	-455.96
methanethiolate	-464.04	2.44	-465.76	-465.55	-467.27
methylphosphonate	-747.22	4.55	-749.81	-750.60	-753.19

(a) Molecular geometries were optimized at the MP2/CVTZ level.

(b) Obtained from CBS extrapolation of the MP2 correlation energy based on Eq. (1) and using the HF/CV5Z energies.

(c) Using an additive combination of electronic energies (CCSD(T)/CVTZ + MP2/CBS – MP2/CVTZ).

Table S1. (cont.)

Ligand	MP2/ CVTZ	ZPVE	CCSD(T)/ CVTZ	MP2/ CBS^(b)	Composite Method^(c)
	D_e		D_e	D_e	D_e
Na (I)					
water	-23.78	1.49	-23.80	-24.75	-24.77
methanol	-25.98	1.08	-25.97	-26.90	-26.89
formic acid	-30.02	1.11	-30.33	-31.09	-31.40
acetic acid	-28.05	0.55	-28.37	-29.13	-29.44
formaldehyde	-25.14	1.12	-25.39	-26.04	-26.30
acetone	-32.35	0.89	-32.63	-33.36	-33.64
formamide	-35.76	1.58	-36.17	-36.81	-37.23
acetamide	-38.34	1.59	-38.76	-39.43	-39.86
<i>N</i> -methyl acetamide	-40.03	1.44	-40.48	-40.67	-41.12
methyl acetate	-31.38	0.86	-31.81	-31.95	-32.38
ammonia	-27.42	1.88	-27.42	-28.44	-28.44
methylamine	-28.63	1.48	-28.67	-29.53	-29.57
methanimine	-29.00	1.41	-28.90	-30.01	-29.92
1H-imidazol	-37.21	1.07	-37.20	-38.27	-38.25
benzene	-25.23	1.12	-25.13	-25.53	-25.43
hydrogen sulfide	-15.51	1.22	-15.44	-16.22	-16.14
methanethiol	-19.48	0.86	-19.41	-20.22	-20.15
hydroxide	-154.69	1.79	-155.67	-156.48	-157.46
metoxi	-150.06	2.55	-150.31	-151.77	-152.03
formiate	-144.02	1.73	-144.73	-146.01	-146.72
acetate	-145.92	1.58	-146.50	-147.93	-148.51
imidazolate- σ	-121.65	1.02	-122.28	-123.14	-123.77
imidazolate- π	-128.45	1.36	-128.63	-129.79	-129.97
hydrosulfide	-130.98	1.03	-131.10	-132.92	-133.04
methanethiolate	-131.30	1.14	-131.39	-133.17	-133.27
methylphosphonate	-236.32	1.85	-237.08	-238.53	-239.29

(a) Molecular geometries were optimized at the MP2/CVTZ level.

(b) Obtained from CBS extrapolation of the MP2 correlation energy based on Eq. (1) and using the HF/CV5Z energies.

(c) Using an additive combination of electronic energies (CCSD(T)/CVTZ + MP2/CBS – MP2/CVTZ).

Table S1. (cont.)

Ligand	MP2/ CVTZ	ZPVE	CCSD(T)/ CVTZ	MP2/ CBS^(b)	Composite Method^(c)
	D_e		D_e	D_e	D_e
Mg (II)					
water	-80.98	1.94	-80.95	-82.72	-82.69
methanol	-94.49	1.26	-94.45	-96.12	-96.08
formic acid	-108.27	1.75	-109.08	-110.23	-111.04
acetic acid	-115.23	0.55	-115.87	-117.29	-117.92
formaldehyde	-91.10	1.78	-91.83	-92.83	-93.56
acetone	-117.65	0.91	-118.32	-119.60	-120.27
formamide	-125.85	2.47	-126.96	-127.80	-128.91
acetamide	-134.70	2.36	-135.70	-136.69	-137.70
<i>N</i> -methyl acetamide	-141.07	2.04	-142.11	-142.62	-143.66
methyl acetate	-119.56	1.14	-120.55	-121.02	-122.01
ammonia	-97.30	2.59	-97.21	-98.78	-98.69
methylamine	-106.83	1.95	-106.79	-108.18	-108.14
methanimine	-105.77	2.16	-105.75	-107.40	-107.38
1H-imidazol	-134.05	1.56	-134.55	-135.72	-136.23
benzene	-119.83	1.53	-119.99	-120.76	-120.92
hydrogen sulfide	-76.34	1.79	-76.42	-77.59	-77.67
methanethiol	-92.32	1.13	-92.50	-93.63	-93.81
hydroxide	-380.92	1.82	-382.67	-383.99	-385.74
metoxi	-378.61	3.81	-378.97	-381.42	-381.78
formiate	-366.95	2.61	-368.58	-370.13	-371.75
acetate	-376.39	2.32	-377.72	-379.63	-380.96
imidazolate- σ	-325.12	1.24	-327.69	-327.38	-329.95
imidazolate- π	-339.64	1.96	-340.61	-341.85	-342.81
hydrosulfide	-347.25	1.55	-348.03	-349.39	-350.17
methanethiolate	-354.70	1.80	-355.56	-356.79	-357.65
methylphosphonate	-587.41	2.95	-588.97	-591.14	-592.71

(a) Molecular geometries were optimized at the MP2/CVTZ level.

(b) Obtained from CBS extrapolation of the MP2 correlation energy based on Eq. (1) and using the HF/CV5Z energies.

(c) Using an additive combination of electronic energies (CCSD(T)/CVTZ + MP2/CBS – MP2/CVTZ).

Table S1. (cont.)

Ligand	MP2/ CVTZ	ZPVE	CCSD(T)/ CVTZ	MP2/ CBS^(b)	Composite Method^(c)
	D_e		D_e	D_e	D_e
K (I)					
water	-17.71	1.28	-17.56	-18.06	-17.92
methanol	-19.36	0.87	-19.15	-19.64	-19.42
formic acid	-23.39	0.89	-23.38	-23.82	-23.80
acetic acid	-20.95	0.41	-20.97	-21.37	-21.39
formaldehyde	-19.29	0.91	-19.22	-19.60	-19.53
acetone	-25.17	0.70	-25.09	-25.51	-25.43
formamide	-27.99	1.32	-28.03	-28.42	-28.46
acetamide	-30.12	1.32	-30.16	-30.57	-30.61
<i>N</i> -methyl acetamide	-31.51	1.17	-31.56	-31.54	-31.59
methyl acetate	-23.93	0.65	-23.97	-23.82	-23.86
ammonia	-19.59	1.53	-19.45	-19.91	-19.77
methylamine	-20.49	1.13	-20.33	-20.64	-20.49
methanimine	-21.26	1.11	-20.94	-21.55	-21.22
1H-imidazol	-28.24	0.80	-27.86	-28.53	-28.15
benzene	-20.06	0.95	-19.00	-19.71	-18.65
hydrogen sulfide	-10.49	0.96	-10.22	-10.75	-10.48
methanethiol	-13.60	0.62	-13.29	-13.85	-13.54
hydroxide	-139.83	1.88	-140.21	-141.60	-141.97
metoxi	-135.45	2.33	-135.15	-137.10	-136.79
formiate	-127.78	1.39	-127.91	-129.22	-129.36
acetate	-129.46	1.25	-129.48	-130.88	-130.89
imidazolate- σ	-106.88	0.67	-106.93	-107.67	-107.72
imidazolate- π	-117.72	1.23	-116.51	-118.70	-117.49
hydrosulfide	-114.25	0.77	-113.83	-116.00	-115.58
methanethiolate	-114.56	0.88	-114.06	-116.19	-115.69
methylphosphonate	-216.59	1.58	-216.53	-218.50	-218.45

(a) Molecular geometries were optimized at the MP2/CVTZ level.

(b) Obtained from CBS extrapolation of the MP2 correlation energy based on Eq. (1) and using the HF/CV5Z energies.

(c) Using an additive combination of electronic energies (CCSD(T)/CVTZ + MP2/CBS – MP2/CVTZ).

Table S1. (cont.)

Ligand	MP2/ CVTZ	ZPVE	CCSD(T)/ CVTZ	MP2/ CBS^(b)	Composite Method^(c)
	D_e		D_e	D_e	D_e
Ca (II)					
water	-55.33	1.73	-54.95	-57.56	-57.19
methanol	-64.84	1.09	-64.31	-67.54	-67.02
formic acid	-78.17	1.50	-78.24	-81.13	-81.19
acetic acid	-79.91	0.43	-79.84	-83.26	-83.18
formaldehyde	-64.43	1.52	-64.45	-66.91	-66.94
acetone	-85.52	0.83	-85.40	-88.85	-88.73
formamide	-92.65	2.19	-92.92	-96.13	-96.40
acetamide	-99.99	2.09	-100.15	-103.80	-103.96
<i>N</i> -methyl acetamide	-105.25	1.81	-105.42	-108.81	-108.99
methyl acetate	-85.85	0.94	-86.05	-88.86	-89.07
ammonia	-63.44	2.17	-63.04	-65.95	-65.55
methylamine	-69.75	1.47	-69.29	-72.60	-72.15
methanimine	-70.34	1.74	-69.78	-73.13	-72.57
1H-imidazol	-93.36	1.20	-92.96	-96.74	-96.34
benzene	-81.03	1.30	-79.35	-84.80	-83.12
hydrogen sulfide	-44.37	1.43	-43.90	-46.62	-46.15
methanethiol	-55.58	0.86	-55.05	-58.28	-57.76
hydroxide	-334.11	2.73	-334.66	-342.40	-342.96
metoxi	-331.50	3.70	-330.63	-340.40	-339.53
formiate	-310.69	2.11	-311.03	-317.83	-318.17
acetate	-318.36	1.86	-318.37	-325.87	-325.88
imidazolate- σ	-273.15	0.99	-272.68	-279.78	-279.32
imidazolate- π	-292.56	1.86	-291.08	-300.33	-298.85
hydrosulfide	-283.59	1.15	-283.05	-291.08	-290.54
methanethiolate	-287.56	1.52	-286.63	-296.80	-295.87
methylphosphonate	-517.66	2.55	-517.40	-528.40	-528.13

(a) Molecular geometries were optimized at the MP2/CVTZ level.

(b) Obtained from CBS extrapolation of the MP2 correlation energy based on Eq. (1) and using the HF/CV5Z energies.

(c) Using an additive combination of electronic energies (CCSD(T)/CVTZ + MP2/CBS – MP2/CVTZ).

Table S2. Energy components (in kcal/mol) of IQA/IQF methodology and classical electrostatic energy calculations by multipolar expansion (ΔE_{multip}^{ML}) for the Li (I), Be (II), Na (I), Mg (II), K (I) and Ca (II) monoligand complexes.

	ΔE^{IQA}	ΔE_{def}^M	ΔE_{def}^L	$\Delta E_{int,class}^{ML}$	$\Delta E_{int,xc}^{ML}$	$\Delta E_{int,disp}^{ML}$	ΔE_{multip}^{ML}
Ligand							
Li (I)							
water	-35.97	2.25	15.11	-39.72	-13.52	-0.09	-36.74
methanol	-39.16	2.88	19.50	-46.22	-14.87	-0.45	-39.04
formic acid	-47.07	3.04	22.38	-56.75	-15.18	-0.55	-43.67
acetic acid	-46.15	3.34	24.72	-57.43	-16.12	-0.80	-42.26
formaldehyde	-39.42	2.60	21.36	-48.72	-14.30	-0.36	-35.05
acetone	-51.42	3.42	23.63	-61.16	-16.47	-0.84	-41.47
formamide	-53.45	3.70	25.47	-65.02	-17.02	-0.57	-50.60
acetamide	-57.37	4.01	26.63	-69.38	-17.88	-0.88	-55.97
<i>N</i> -methyl acetamide	-59.50	4.21	25.63	-72.34	-18.38	-1.18	-52.56
methyl acetate	-50.49	3.67	25.97	-62.12	-16.90	-1.11	-44.97
ammonia	-40.15	1.38	17.15	-44.01	-14.55	-0.12	-57.29
methylamine	-42.20	1.85	19.64	-47.94	-15.29	-0.47	-47.29
methanimine	-43.39	1.92	20.61	-50.39	-15.18	-0.35	-44.70
1H-imidazol	-53.10	2.65	24.98	-63.18	-16.70	-0.86	-54.54
benzene	-39.29	-4.14	31.63	-45.50	-20.47	-0.81	-12.26
hydrogen sulfide	-23.65	-1.84	17.75	-28.66	-10.58	-0.32	-17.76
methanethiol	-28.88	-1.55	20.48	-35.76	-11.82	-0.68	-23.54
hydroxide	-191.48	8.19	19.45	-189.77	-29.31	-0.04	-193.72
metoxi	-185.02	7.94	23.13	-186.11	-29.51	-0.47	-151.94
formiate	-171.61	5.71	25.04	-175.79	-26.38	-0.18	-187.45
acetate	-173.48	6.23	28.73	-180.53	-27.43	-0.48	-182.92
imidazolate- σ	-147.75	5.33	25.04	-154.87	-22.41	-0.84	-168.45
imidazolate- π	-154.04	-1.68	23.61	-145.94	-29.73	-0.30	-145.71
hydrosulfide	-151.17	-0.02	20.36	-150.46	-20.96	-0.09	-180.19
methanethiolate	-152.60	0.16	21.97	-152.86	-21.60	-0.53	-169.84
methylphosphonate	-279.61	7.95	23.85	-277.61	-34.77	-1.12	-362.29

Table S2. (cont.)

Ligand	ΔE^{IQA}	ΔE_{def}^M	ΔE_{def}^L	$\Delta E_{int,class}^{ML}$	$\Delta E_{int,xc}^{ML}$	$\Delta E_{int,disp}^{ML}$	ΔE_{multip}^{ML}
Be (II)							
water	-147.05	-33.95	88.46	-165.02	-35.95	-0.59	-128.92
methanol	-175.49	-39.69	142.80	-233.14	-43.93	-1.53	-156.07
formic acid	-196.84	-41.25	144.37	-254.14	-44.90	-0.92	-159.02
acetic acid	-209.04	-51.56	167.93	-268.19	-49.63	-0.93	-147.55
formaldehyde	-173.21	-39.46	130.55	-221.51	-42.00	-0.78	-113.95
acetone	-213.62	-44.69	155.47	-274.56	-48.27	-1.57	-78.95
formamide	-220.18	-44.36	149.03	-275.35	-48.34	-1.14	-151.89
acetamide	-232.37	-46.28	156.81	-290.92	-50.48	-1.63	-206.62
<i>N</i> -methyl acetamide	-242.99	-47.54	159.69	-303.58	-51.99	-2.12	-81.49
methyl acetate	-217.59	-45.29	164.12	-284.79	-49.69	-1.93	-137.59
ammonia	-169.77	-43.26	95.39	-182.42	-38.51	-0.97	-101.37
methylamine	-186.86	-46.04	116.17	-213.15	-41.79	-2.05	-149.05
methanimine	-190.17	-45.72	123.02	-223.65	-42.59	-1.23	-144.96
1H-imidazol	-227.98	-50.48	151.14	-278.66	-47.86	-2.11	-197.56
benzene	-229.12	-112.40	204.07	-249.46	-68.53	-2.79	27.75
hydrogen sulfide	-141.78	-70.98	124.59	-153.39	-40.58	-1.41	-67.99
methanethiol	-165.90	-77.17	142.50	-185.25	-44.72	-1.72	-87.49
hydroxide	-515.55	-55.72	97.39	-493.91	-62.95	-0.35	-433.83
metoxi	-515.99	-61.80	122.82	-508.97	-66.78	-1.25	-469.04
formiate	-491.57	-60.86	145.84	-513.41	-62.72	-0.42	-619.45
acetate	-505.13	-62.21	160.45	-537.43	-65.39	-0.55	-587.54
imidazolate- σ	-447.31	-65.71	150.54	-469.94	-60.06	-2.14	-565.41
imidazolate- π	-471.14	-112.09	162.26	-442.61	-77.26	-1.44	-320.31
hydrosulfide	-449.16	-100.46	120.67	-407.40	-61.51	-0.45	-647.02
methanethiolate	-462.37	-108.72	131.55	-418.69	-65.57	-1.20	-407.14
methylphosphonate	-758.19	-72.09	171.87	-780.05	-79.03	-0.99	-989.70

Table S2. (cont.)

Ligand	ΔE^{IQA}	ΔE_{def}^M	ΔE_{def}^L	$\Delta E_{int,class}^{ML}$	$\Delta E_{int,xc}^{ML}$	$\Delta E_{int,disp}^{ML}$	ΔE_{multip}^{ML}
Na (I)							
water	-24.73	2.91	10.52	-25.99	-11.80	-0.37	-24.95
methanol	-26.18	3.42	13.73	-29.54	-12.85	-0.93	-26.18
formic acid	-33.43	4.20	15.51	-38.93	-13.33	-0.87	-31.49
acetic acid	-31.94	4.47	21.64	-42.79	-14.13	-1.12	-35.86
formaldehyde	-27.82	3.83	14.21	-32.71	-12.43	-0.72	-25.49
acetone	-37.10	4.72	15.27	-41.52	-14.33	-1.24	-31.84
formamide	-38.11	5.04	17.31	-44.66	-14.90	-0.90	-36.65
acetamide	-40.54	5.42	18.66	-47.84	-15.66	-1.25	-39.60
<i>N</i> -methyl acetamide	-42.10	5.64	17.25	-49.85	-16.08	-1.60	-40.11
methyl acetate	-35.50	4.89	17.13	-41.31	-14.69	-1.52	-33.99
ammonia	-27.00	0.97	13.31	-27.08	-13.76	-0.44	-30.23
methylamine	-28.39	1.23	14.85	-29.03	-14.40	-1.04	-31.06
methanimine	-29.78	1.79	15.12	-31.69	-14.17	-0.82	-30.04
1H-imidazol	-37.25	2.51	18.47	-40.95	-15.83	-1.45	-36.94
benzene	-25.38	0.08	19.47	-27.89	-15.31	-1.73	-14.30
hydrogen sulfide	-15.57	-1.74	12.91	-15.69	-10.19	-0.86	-11.72
methanethiol	-19.72	-1.68	14.71	-20.41	-11.61	-1.19	-15.44
hydroxide	-158.02	11.47	15.15	-157.40	-27.08	-0.16	-153.98
metoxi	-151.80	11.26	17.50	-152.95	-26.87	-0.74	-155.84
formiate	-145.75	8.06	17.99	-143.69	-27.63	-0.47	-158.40
acetate	-146.73	8.65	20.50	-146.78	-28.33	-0.77	-158.84
imidazolate- σ	-123.56	4.63	17.70	-121.05	-23.44	-1.39	-131.38
imidazolate- π	-127.80	5.05	16.15	-123.51	-24.56	-0.93	-121.12
hydrosulfide	-129.21	-3.68	14.41	-113.86	-25.78	-0.30	-143.96
methanethiolate	-130.58	-3.87	14.79	-114.26	-26.59	-0.91	-141.00
methylphosphonate	-241.84	12.44	14.66	-234.14	-35.53	-1.36	-287.56

Table S2. (cont.)

	ΔE^{IQA}	ΔE_{def}^M	ΔE_{def}^L	$\Delta E_{int,class}^{ML}$	$\Delta E_{int,xc}^{ML}$	$\Delta E_{int,disp}^{ML}$	ΔE_{multip}^{ML}
Ligand							
Mg (II)							
water	-83.36	-14.36	44.48	-84.74	-27.13	-1.60	-69.22
methanol	-96.71	-16.44	62.95	-109.36	-31.43	-2.42	-79.52
formic acid	-115.05	-12.16	73.75	-143.09	-32.49	-1.05	-89.64
acetic acid	-116.57	-21.90	86.75	-142.40	-37.80	-1.21	-108.46
formaldehyde	-98.61	-11.75	65.94	-121.61	-30.21	-0.99	-70.33
acetone	-124.65	-12.78	80.22	-155.29	-34.79	-2.00	-85.21
formamide	-130.05	-12.64	78.93	-159.60	-35.34	-1.40	-102.69
acetamide	-139.23	-12.95	82.56	-170.03	-36.90	-2.05	-112.55
<i>N</i> -methyl acetamide	-145.49	-13.25	84.48	-178.58	-37.99	-2.69	-108.94
methyl acetate	-126.09	-13.23	85.31	-159.80	-35.95	-2.42	-97.18
ammonia	-98.18	-31.52	53.39	-84.39	-33.18	-2.48	-82.47
methylamine	-107.19	-35.89	65.54	-97.00	-36.50	-3.34	-93.14
methanimine	-109.44	-31.04	67.69	-108.39	-35.73	-1.98	-85.03
1H-imidazol	-134.90	-32.73	83.73	-143.26	-40.00	-2.63	-107.70
benzene	-120.10	-48.98	109.63	-131.12	-46.29	-3.33	-25.96
hydrogen sulfide	-76.13	-52.89	70.99	-58.55	-33.80	-1.88	-35.34
methanethiol	-92.69	-60.88	82.01	-73.53	-38.46	-2.29	-45.18
hydroxide	-387.77	-15.29	52.11	-373.31	-50.45	-0.84	-369.29
metoxi	-381.69	-18.35	66.44	-375.93	-52.37	-1.47	-332.45
formiate	-370.11	-29.26	73.56	-357.88	-56.05	-0.47	-379.81
acetate	-376.84	-29.18	84.24	-373.04	-58.16	-0.70	-376.55
imidazolate- σ	-325.55	-50.05	80.47	-300.63	-52.72	-2.63	-324.13
imidazolate- π	-339.60	-42.95	86.26	-325.75	-55.07	-2.10	-292.28
hydrosulfide	-342.32	-99.74	60.03	-240.10	-61.58	-0.93	-350.13
methanethiolate	-350.57	-113.06	65.01	-235.35	-65.89	-1.55	-323.76
methylphosphonate	-593.15	-29.31	87.68	-581.31	-71.38	-0.91	-721.29

Table S2. (cont.)

Ligand	ΔE^{IQA}	ΔE_{def}^M	ΔE_{def}^L	$\Delta E_{int,class}^{ML}$	$\Delta E_{int,xc}^{ML}$	$\Delta E_{int,disp}^{ML}$	ΔE_{multip}^{ML}
K (I)							
water	-18.10	4.30	8.89	-19.29	-11.30	-0.70	-17.79
methanol	-19.08	5.00	11.30	-21.56	-12.49	-1.33	-18.40
formic acid	-25.86	5.79	12.80	-29.94	-13.31	-1.19	-23.92
acetic acid	-22.41	6.33	20.49	-33.51	-14.30	-1.42	-27.16
formaldehyde	-20.66	5.17	12.15	-24.64	-12.27	-1.07	-19.10
acetone	-28.41	6.49	13.08	-31.85	-14.58	-1.54	-24.29
formamide	-28.72	7.01	15.59	-34.74	-15.38	-1.20	-27.83
acetamide	-30.33	7.58	17.27	-37.44	-16.34	-1.52	-30.04
<i>N</i> -methyl acetamide	-31.92	7.91	15.28	-38.90	-16.88	-1.88	-30.68
methyl acetate	-27.04	6.61	13.88	-30.97	-14.77	-1.80	-33.91
ammonia	-19.08	3.06	10.43	-19.29	-12.50	-0.79	-20.66
methylamine	-19.64	3.60	11.89	-20.47	-13.18	-1.48	-20.60
methanimine	-21.54	3.85	11.86	-22.92	-13.10	-1.22	-20.88
1H-imidazol	-28.05	5.06	14.57	-30.69	-15.11	-1.88	-26.29
benzene	-18.40	1.87	15.62	-17.01	-16.21	-2.65	-16.27
hydrogen sulfide	-10.97	0.16	8.63	-9.86	-8.46	-1.44	-7.59
methanethiol	-13.78	0.63	10.04	-13.53	-9.81	-1.57	-10.30
hydroxide	-139.50	20.86	18.88	-144.02	-35.00	-0.22	-145.42
metoxi	-134.11	20.31	20.00	-139.05	-34.45	-0.91	-139.40
formiate	-127.21	15.86	19.45	-129.58	-32.14	-0.79	-137.91
acetate	-127.22	16.62	22.32	-132.04	-33.05	-1.07	-138.62
imidazolate- σ	-106.75	11.56	17.06	-108.44	-25.17	-1.75	-111.13
imidazolate- π	-113.30	9.71	15.38	-105.12	-31.78	-1.49	-111.16
hydrosulfide	-111.05	5.36	13.01	-102.69	-26.21	-0.52	-121.17
methanethiolate	-112.21	6.20	13.26	-104.33	-26.66	-0.95	-119.67
methylphosphonate	-218.00	25.04	16.59	-215.26	-44.88	-1.58	-250.36

Table S2. (cont.)

Ligand	ΔE^{IQA}	ΔE_{def}^M	ΔE_{def}^L	$\Delta E_{int,class}^{ML}$	$\Delta E_{int,xc}^{ML}$	$\Delta E_{int,disp}^{ML}$	ΔE_{multip}^{ML}
Ca (II)							
water	-56.01	-5.65	32.93	-55.14	-26.32	-1.83	-49.31
methanol	-64.77	-6.55	45.73	-70.01	-31.41	-2.54	-55.34
formic acid	-81.49	-4.92	57.15	-97.38	-35.16	-1.17	-67.73
acetic acid	-84.41	-5.32	69.10	-108.46	-37.89	-0.73	-86.76
formaldehyde	-68.44	-5.01	49.92	-80.36	-31.90	-1.08	-77.32
acetone	-89.06	-5.89	63.19	-105.38	-38.74	-2.23	-67.45
formamide	-93.08	-5.87	63.75	-109.49	-39.94	-1.53	-79.07
acetamide	-99.01	-6.28	69.73	-117.84	-42.51	-2.25	-85.56
<i>N</i> -methyl acetamide	-105.85	-6.50	69.31	-123.86	-44.30	-3.04	-87.52
methyl acetate	-88.50	-5.90	68.04	-107.66	-40.21	-2.76	-73.04
ammonia	-63.28	-13.14	36.75	-55.01	-29.05	-2.82	-59.97
methylamine	-69.07	-13.96	44.56	-64.02	-32.24	-3.39	-63.24
methanimine	-71.52	-12.48	47.11	-71.48	-32.54	-2.12	-59.85
1H-imidazol	-91.20	-13.17	61.64	-98.72	-38.59	-2.35	-76.54
benzene	-76.52	-36.57	73.77	-63.40	-47.43	-2.90	-42.12
hydrogen sulfide	-43.09	-21.56	40.73	-35.77	-24.83	-1.65	-22.62
methanethiol	-54.23	-23.59	49.06	-49.30	-28.73	-2.13	-30.08
hydroxide	-333.88	-9.39	48.43	-301.62	-70.48	-0.82	-331.83
metoxi	-327.17	-11.80	59.11	-299.28	-73.58	-1.61	-320.25
formiate	-307.96	-12.14	61.85	-289.92	-67.32	-0.41	-330.36
acetate	-313.45	-12.03	70.31	-300.15	-70.43	-0.56	-333.05
imidazolate- σ	-267.07	-20.60	67.41	-250.84	-61.47	-1.58	-261.08
imidazolate- π	-284.69	-39.04	58.43	-231.83	-70.40	-1.85	-249.05
hydrosulfide	-276.76	-42.06	42.99	-220.53	-56.16	-0.98	-286.19
methanethiolate	-281.14	-39.05	55.89	-235.01	-62.28	-0.95	-247.34
methylphosphonate	-514.69	-15.22	67.47	-473.77	-94.29	-0.96	-615.64

Table S3. Change of IQA additive atomic energies (in kcal/mol) for the metals M: Li (I), Be (II), Na (I), Mg (II), K (I) and Ca(II) and several selected monoligand complexes.

Element	Li (I)	Be (II)	Na (I)	Mg (II)	K (I)	Ca (II)
Methanol						
M	-27.89	-178.99	-18.24	-88.05	-12.69	-58.53
O	-114.73	-281.79	-94.36	-225.99	-80.85	-190.88
H	51.07	129.16	42.65	105.58	36.66	90.43
C	35.93	40.27	33.84	52.51	31.63	54.80
H	1.83	31.72	-0.27	10.14	-1.33	2.89
H	7.32	42.07	5.10	24.55	3.75	18.26
H	7.32	42.07	5.10	24.55	3.75	18.26
<i>N</i> -methyl acetamide						
M	-41.73	-226.38	-28.13	-122.88	-20.92	-92.10
C	8.72	27.96	7.43	20.73	6.62	17.98
C	101.42	204.62	89.07	185.49	81.97	172.93
O	-119.25	-276.86	-99.82	-231.41	-87.38	-198.99
N	-80.86	-176.25	-71.68	-156.08	-65.98	-145.95
C	24.75	43.49	23.87	43.49	22.26	43.40
H	26.88	70.34	23.21	57.51	20.95	52.00
H	4.10	18.81	3.09	13.53	2.52	11.14
H	3.30	14.59	2.05	8.70	1.41	6.68
H	3.30	14.59	2.05	8.70	1.41	6.68
H	5.43	20.66	4.40	15.86	3.74	13.88
H	0.95	9.45	-0.10	4.16	-0.54	1.99
H	0.95	9.45	-0.10	4.16	-0.54	1.99
Methylamine						
M	-29.99	-174.53	-21.01	-104.31	-13.97	-63.79
N	-114.04	-318.59	-91.89	-238.46	-76.75	-194.26
H	31.87	96.54	26.34	73.41	22.03	58.76
H	31.87	96.54	26.34	73.41	22.03	58.76
C	28.50	41.06	26.95	45.80	25.47	45.86
H	1.63	20.17	0.06	10.02	-1.04	3.70
H	1.63	20.17	0.06	10.02	-1.04	3.70
H	6.33	31.77	4.74	22.93	3.65	18.21

Table S3. (cont.)

Atom	Li (I)	Be (II)	Na (I)	Mg (II)	K (I)	Ca (II)
Benzene						
M	-37.53	-272.80	-22.38	-139.35	-16.06	-93.43
C	-9.99	-34.06	-6.96	-25.40	-4.82	-17.52
C	-9.99	-33.93	-6.96	-25.40	-4.98	-17.52
C	-9.98	-33.92	-6.92	-25.10	-4.90	-17.28
C	-9.98	-33.98	-6.92	-25.10	-4.74	-17.44
C	-9.98	-33.85	-6.92	-25.10	-4.90	-17.44
C	-9.98	-33.92	-6.92	-25.10	-4.90	-17.28
H	9.70	41.22	6.43	28.42	4.51	20.24
H	9.70	41.24	6.43	28.42	4.49	20.24
H	9.68	41.22	6.44	28.40	4.47	20.23
H	9.68	41.21	6.44	28.40	4.49	20.22
H	9.69	41.22	6.44	28.40	4.48	20.23
H	9.69	41.22	6.44	28.40	4.47	20.23
Methanethiol						
M	-25.68	-193.01	-18.28	-118.02	-11.82	-63.67
S	-31.20	-124.59	-19.91	-76.19	-12.14	-62.23
H	5.76	50.00	1.15	30.54	-3.40	18.30
C	4.28	16.03	3.65	10.77	3.41	10.64
H	5.15	26.75	3.66	17.98	2.36	11.69
H	8.19	33.29	6.65	25.63	5.16	19.33
H	4.16	25.17	2.90	16.15	2.20	11.24
Acetate						
Me	-97.99	-363.90	-79.29	-245.13	-66.45	-197.66
C	1.06	19.35	0.72	13.19	0.51	9.46
C	144.83	304.43	127.74	267.93	118.27	248.97
O	-110.34	-252.17	-96.57	-216.77	-87.94	-193.23
O	-110.52	-252.35	-96.75	-216.95	-88.12	-193.41
H	-0.08	16.24	0.55	9.28	0.16	6.35
H	-0.95	11.63	-1.56	5.80	-1.83	3.27
H	0.50	11.63	-1.56	5.80	-1.83	3.27

Figure S1. MP2/CVTZ optimized structures of the considered metal-ligand complexes.

Li(I) complexes

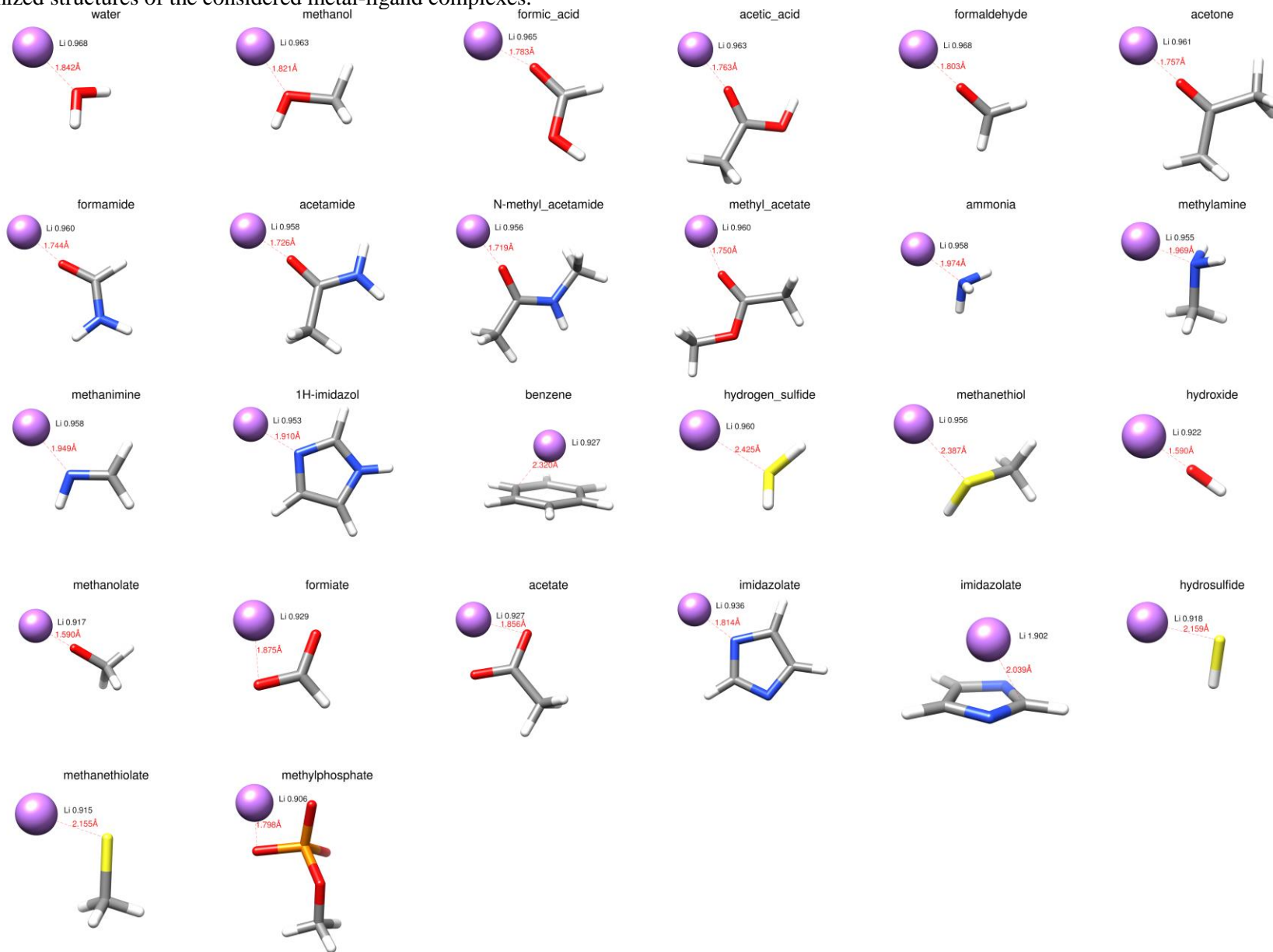


Figure S1. (cont.)

**Na(I)
complexes**

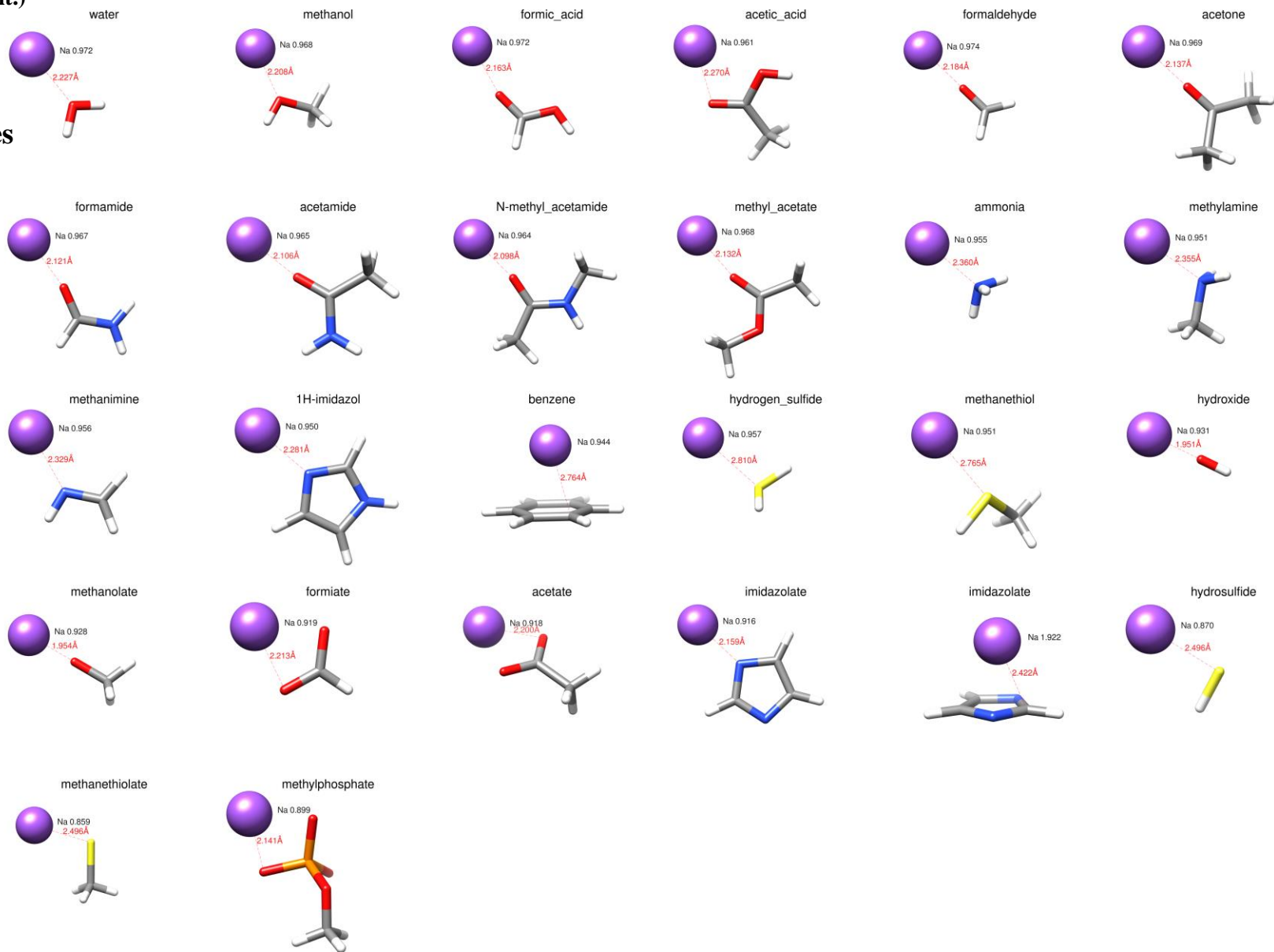


Figure S1. (cont.)

**K(I)
complexes**

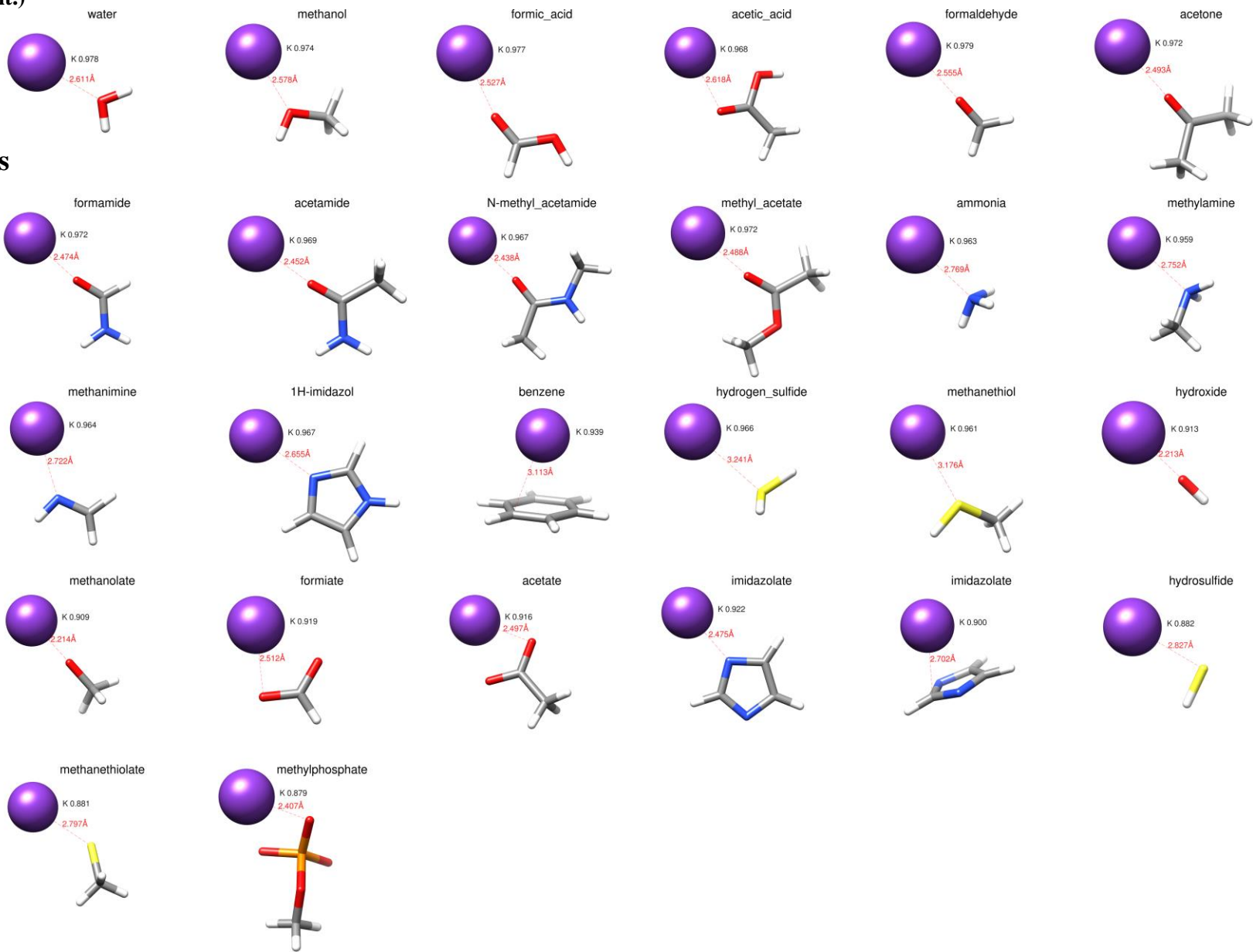


Figure S1. (cont.)

**Be(II)
complexes**

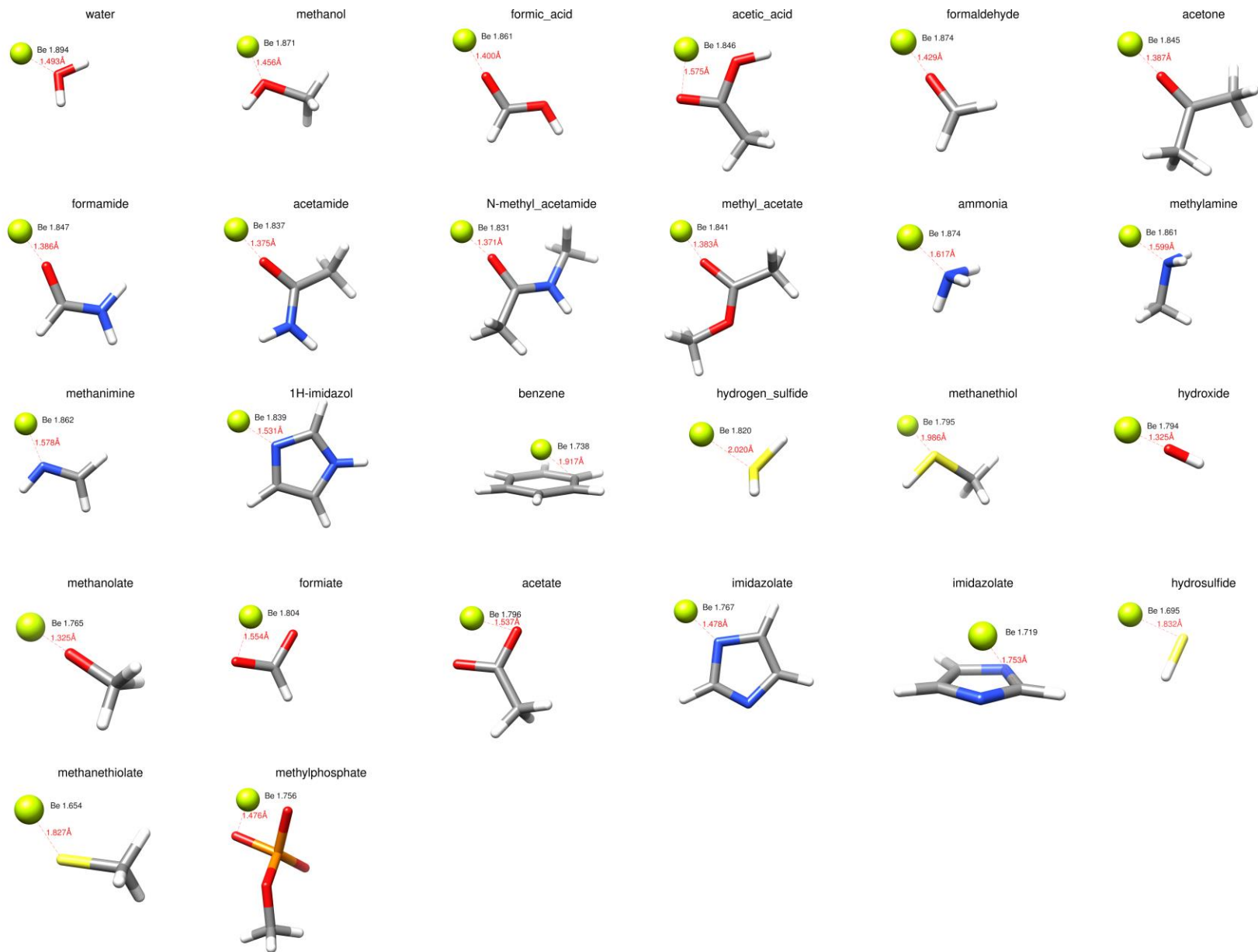


Figure S1. (cont.)

Mg(II)
complexes

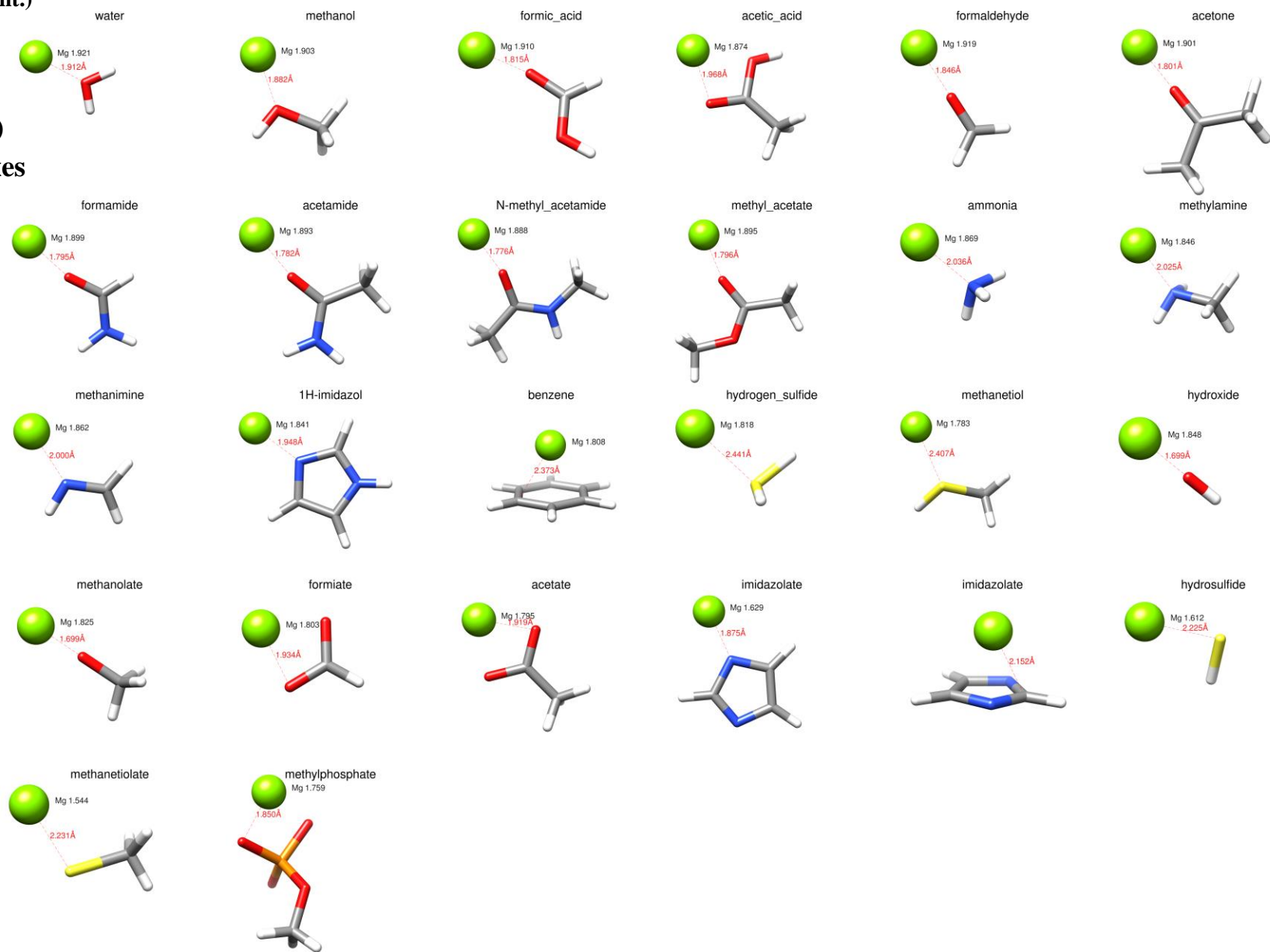


Figure S1. (cont.)

Ca(II)
complexes

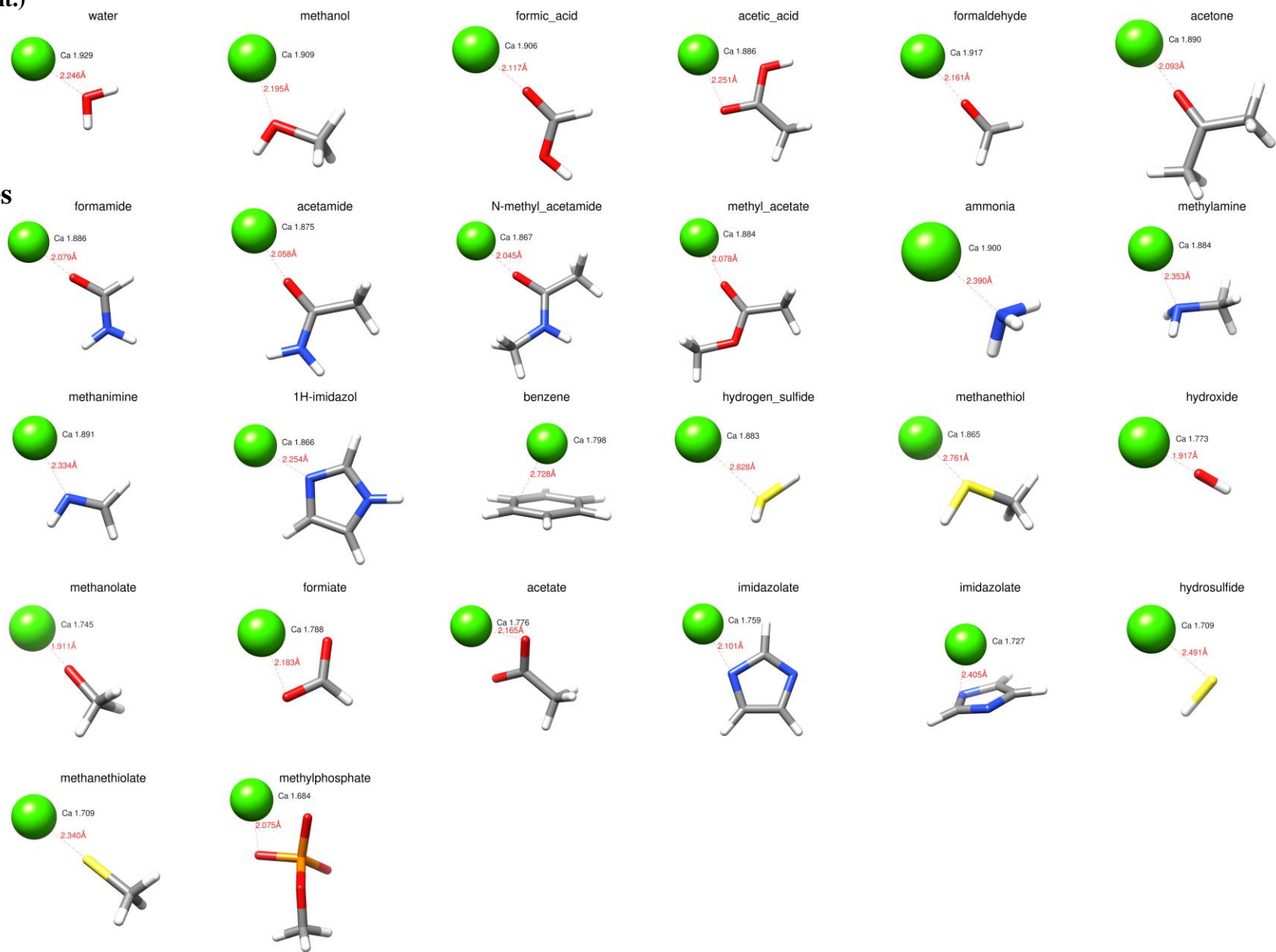


Figure S2. Histograms showing the ligand→metal charge transfer (Δq in e^-) computed from the NPA atomic charges and using the MP2/CVTZ density.

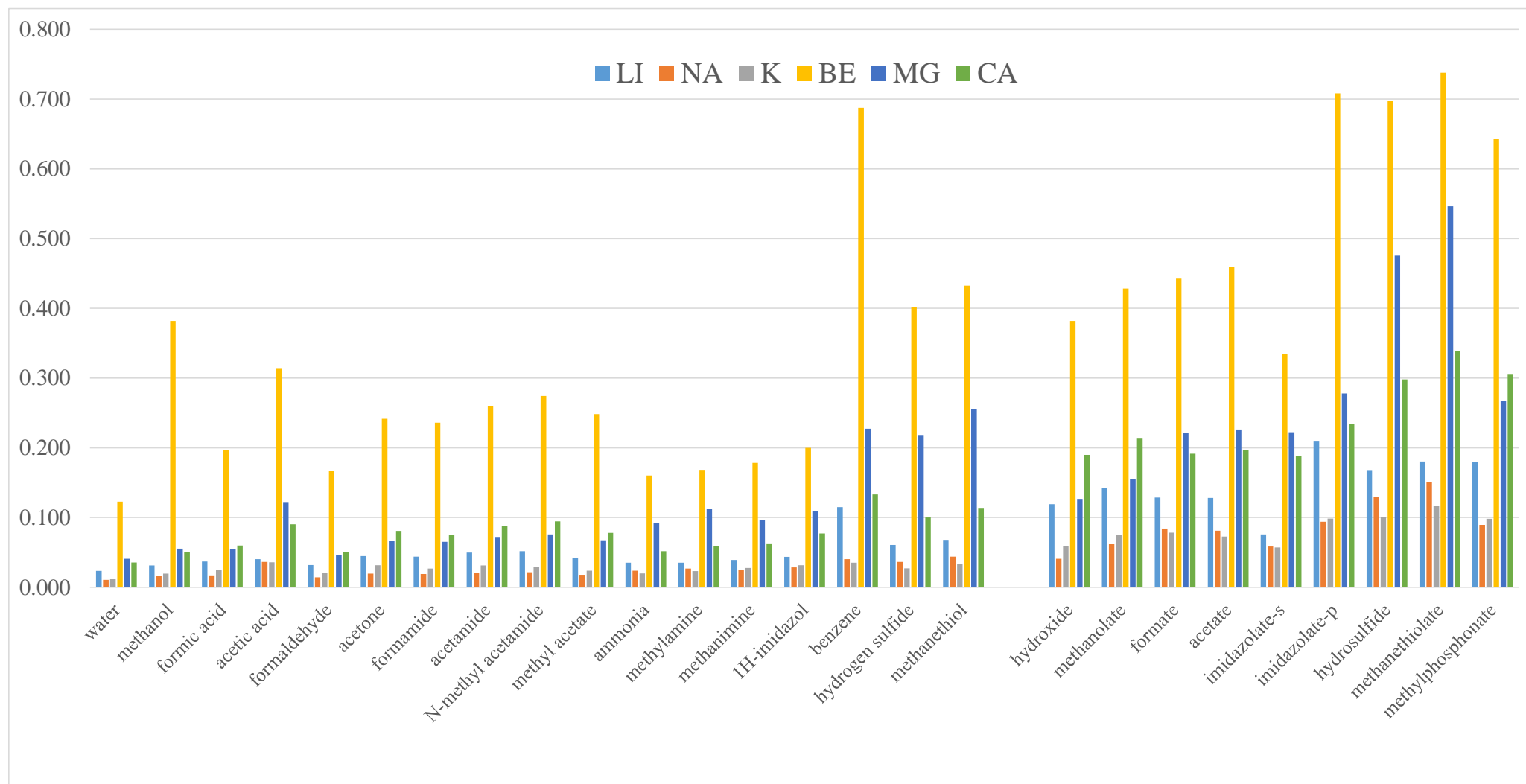


Figure S3. Comparison between the HF-D3/CVTZ bond energies (ΔE in kcal/mol) and the benchmark composite bond energies (D_e) of the metal-ligand complexes. The determination coefficient (R^2), the Spearman correlation coefficient (ρ) and the root mean square (RMS) error in kcal/mol are also indicated for the whole data set (in black) and for the monoanionic ligand (in blue) and the neutral ligand (in red). The blue dashed line is the least squared fit line between the calculated and the reference data.

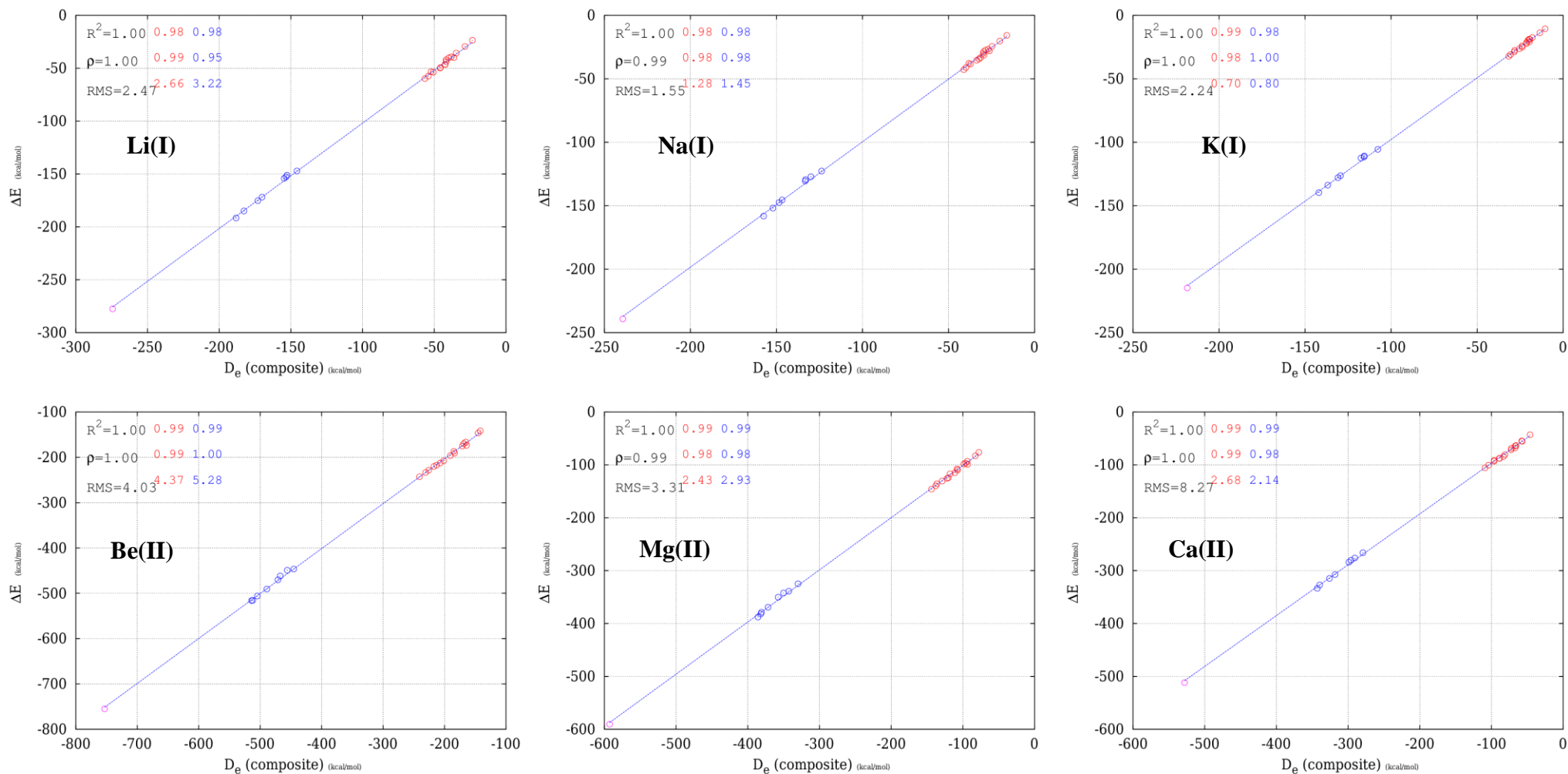


Figure S4. Histogram showing the strain energies of the ligand molecules computed at the HF-D3/CVTZ level.

